Charmed Baryon Spectroscopy via the (π, D^{*-}) reaction

Y. Morino, T. Nakano,* H. Noumi†,* K. Shirotori, Y. Sugaya, and T. Yamaga
Research Center for Nuclear Physics (RCNP), Osaka University,
10-1 Mihogaoka, Ibaraki, Osaka 567-0047, Japan

K. Ozawa‡
Institute of Particle and Nuclear Studies(IPNS),
High Energy Accelerator Research Organization (KEK),
1-1 Oho, Tsukuba, Ibaraki 305-0801, Japan

T. Ishikawa
Reserach Center for Electron Photon Science,
Tohoku University, 1-2-1, Mikamine,
Taihaku-ku, Sendai, Miyagi 982-0826, Japan

Y. Miyachi
Physics Department, Yamagata University,
1-4-12 Kojirakawa-machi, Yamagata 990-8560, Japan

K. Tanida
Department of Physics and Astronomy,
Seoul National University, Seoul 151-747, Korea

---

† Spokesperson

‡ Co-Spokesperson

*alternative affiliation: IPNS, KEK, 1-1, Oho, Tsukuba, Ibaraki 305-0801, Japan

Executive Summary

We propose a spectroscopic study of charmed baryons via the (π, D^{*-}) reactions at the high-momentum (high-p) beam line of J-PARC to investigate the diquark degrees of freedom in a hadron. Good diquark correlation is due to the color–spin interaction whose strength is proportional to the inverse of quark mass. Therefore, there would be only one good diquark pair in a charmed baryon, which makes the study of excited charmed baryons unique and interesting.

We will supplement the high-p beam line with dispersive ion optical elements so that a high-intensity pion beam with a resolution of $\Delta p/p$=0.1 % can be delivered. A new large acceptance spectrometer for D^{*-} detection is designed to achieve a missing mass resolution of ∼5 MeV. Charmed baryons from the ground state to highly excited states of $E_x \sim 1$ GeV will be identified in the missing mass spectrum of the $p(\pi, D^{*-})$ reaction. In addition to determining the masses and widths of charmed baryons, the spectrometer enables us to measure some of the decay branching ratios of an excited baryon by detecting decay products.

Based on our developments of the beam line system, we propose a new charmed baryon spectroscopy by means of the missing mass method to investigate diquarks.

I. INTRODUCTION

Although we know the fundamental law of the strong interaction, quantum chromodynamics (QCD), the dynamics of hadrons at low energy is not easily described in terms of the bare quarks and gluons. As being strongly correlated systems, the construction of hadrons may require good insight with more ingredients beyond the bare particles. The possible formation of various kinds of active constituents at relevant energy scale as quasi-particles is the origin of the variety of hadrons.

Due to the strong interaction effects, light u, d and s quarks are renormalized to emerge as quasi-particles and become active building blocks of hadrons at low energy. Thus dressed quarks are referred to as constituent quarks. Contrary, heavy charm and bottom quarks are almost good constituents by themselves. The strongly renormalized u, d and s quarks and almost bare c and b quarks are the basic building blocks of hadrons that we shall study. The quark model based on these quarks have been generally successful especially for the ground state hadrons [1]. It also describes an important feature of the nuclear force [2].

Yet, problems have been recognized among resonances. For instance; (1) not all quark model states are observed, which is known as the missing resonance problem, and (2) many resonances above decay channel threshold are not well described. The so-called exotic hadrons are particularly so.

Diquarks have been discussed in hadron physics for a long time [7–10]. There are many phenomenological suggestions or even "evidence" of diquarks. The above-mentioned missing resonance problem in baryons might be solved by introducing diquarks. Exotic hadrons such as "light-narrow" penta-quark state are explained as a positive parity state by diquark picture, togather with the "lightest" positive partity nucleon resonance, Roper [9]. Ref. [9] discusses also why the lightest scalar meson nonet appears below 1 GeV with a diquark model.

The so-called good diquark is formed due to strong attraction in the color-spin (color-magnetic) interaction between two quarks (Appendix A). In baryonic system with light quarks, the effect of the good diquark correlations may be difficult to see because 3 pairs of diquark correlations are at equal weight. If a light quark is replaced by a heavy quark in a baryon, because the color-spin interection is proportional to the inverse of a quark mass (Eq. A3), the other two light quarks are expected to correlate strongly, thus, may develope a diquark. Lattice QCD calculations demonstrate strong spatial correlations between two light quarks with a spin-singlet, color antitriplet configuration in a baryon with introducing a static quark[11, 12]. A charm quark would act as a static quark and may isolate the other two light quarks. If the isolated two light quarks make a collective system, a relative motion in the light quarks (ρ mode) and a collective motion of them to the heavy quark (λ mode) may split in excited states, as illustrated in Fig. 1. If this is the case, characteristic patterns of the level structure of excited states, such as Regge trajectories, might be seen. A diquark mass may be determined from a slope parameter of a Regge trajectory. Although this is

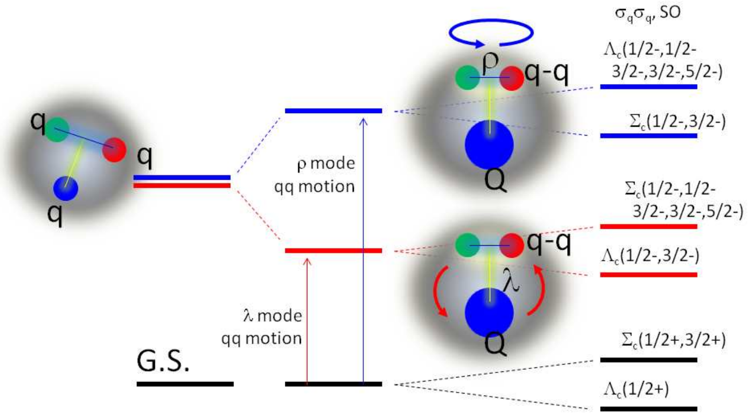

FIG. 1: Schematic picture of quark correlations in a baryon. In a baryon with light quarks, the correlations are equal weight and the orbital excitation levels are degenerated, as illustrated in the left hand side. In the case that two light quarks make a collective system by introducing a heavy quark in a baryon, the orbtal excitation could be split into a relative orbital motion between two light quarks and a collective motion of the light quarks relative to the heavy quark(right).

a naive picture, the pattern, if it is found, must carry infomation on a strongly correlated colored object, the dynamics of which should be explained by QCD. One considers the case that a string tension between quarks becomes large enough to create a $q\bar{q}$ pair in a excited state. In a light baryon system, a light meson (Nambu-Goldstone boson) will be easily created at one end of the string with q, forming a lighter baryon at the other end of the string with "qq". If a light qq pair forms a diquark in a charmed baryon, a string between the diquark and a charm quark will be expanded at an excited state. This may favor a decay to $Q\bar{q}$ and qqq (if it opens energetically) and suppress a decay to Qqq and $q\bar{q}$. This may one of explanations for narrow widths of the charmed baryons.

In this respect, a charmed baryon with a charm quark (Y_c) provides a unique opportunity to look into quark dynamics, particularly diquarks and/or diquark correlations, in hadrons. Giving information on a structure in a hadron, we could further understand QCD in non-perturbative region. However, a limited number of charmed baryons are reported to date. Therefore, a systematic measurement of a charmed baryon is strongly desired.

We will measure charmed baryons via the (π, D^{*-}) reactions, where the charmed baryons are identified in missing mass spectra. We will supplement the high-momenum (hipgh-p) beam line at J-PARC with dispersive ion optical elements so that a high-intenisty pion beam with a resolution of $\Delta p/p$=0.1 % can be delivered (Section refsec-hpbl. A new large acceptnce spectrometer for the D^{*-} detection is designed to achieve a missing mass resolution of as good as 5 MeV, as described in Section III B. Charmed baryons from the ground state to highly excited states of the excitation energy equal to ∼1 GeV will be identified in a missing mass spectrum of the $p(\pi, D^{*-})$ reaction. Expected missing mass spectrum is demonstrated

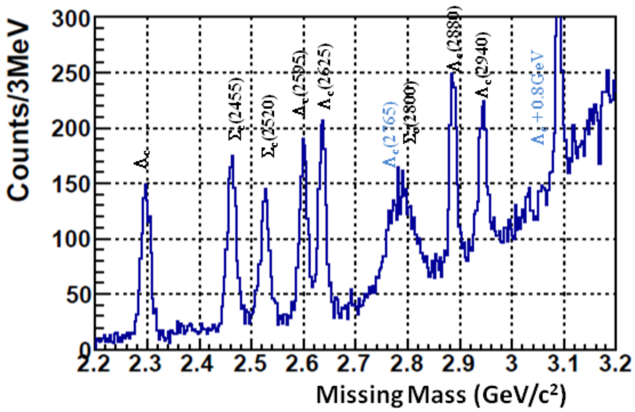

FIG. 2: Missing mass spectrum of the (π, D^{*-}) reaction on hydrogen is demonstrated by a Monte Calro simulation. Here, known states reported by Particle Data Group [3] are taken into account, except for the highest peak at ∼3.08 GeV/c^2, assuming a production cross section for each state to be 1 nb.

in Fig. 2. Here, known states reported by the Particle Data Group [3] are taken into account, except for the highest peak at ∼3.08 GeV/c^2, assuming the production cross section for each state to be 1 nb. A number of background events can be reduced by identifying a charmed meson production twice, namely D^{*-} and D^0 in a decay chain of $D^{*-} \rightarrow \bar{D}^0 + \pi^-$ followed by $\bar{D}^0 \rightarrow K^+\pi^-$. Details are described in Section III B.

We will measure the excitation energies and widths of the charmed baryon states, in which we expect to find some hither-to-unobserved states. We could deduce informtion on a diqaurk correlation from the measured level structure. In addition to the masses and widths, the spectrometer enables us to measure some of decay branching ratios of a excited baryon by detecting decay products(Section III B). Decay branching ratios (partial decay widths) can be immediately obtained from the numbers of produced parent and daughter states populated via the (π, D^{*-}) and $(\pi, D^{*-}M)$ reactions, respectively, where M represents the decay particles from a polulated charmed baryon. This is an advantage of the missing mass spectroscopy. According to the simulation, angular range of the decay particle can be covered widely so as to measure an angular distribution. This as well as the decay branching ratio would be helpful to determine a spin of the state [13, 14]. The production cross section must carry information on structure of produced charmed baryon through the coupling constant and transition form factor at the NDY_c and/or ND^*Y_c vertices.

Here, we propose new charmed baryon spectroscopy by means of the missing mass method to shed lights on the diquark.

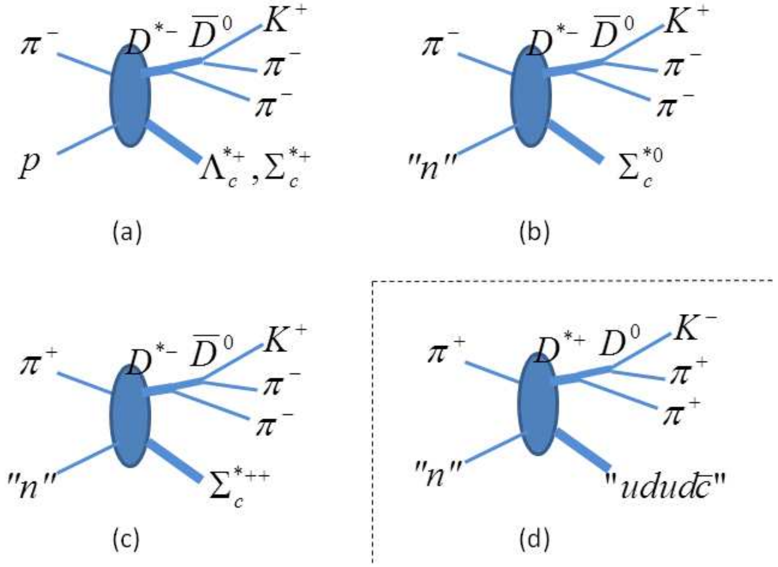

FIG. 3: Diagrams of the reactions and decays considered in the study.

II. $(\pi, \bar{D}^{*-})$ REACTION

We propose to study charmed baryons at the high momentum beam line of the J-PARC hadron facility. Charmed baryons will be identified in the missing mass spectra of (π, D^{*-}) reactions. Charmed baryons can be produced in a wide mass range simultaneously, from the ground state up to highly excited states of excitation energy as high as 1 GeV. In the standard set up, the (π^-, D^{*-}) reaction on a hydrogen target can populate both Λ_c^{*+} and Σ_c^{*+}, as illustrated in Fig. 3-(a). By changing the beam polarity and/or the target (e.g. neutron in deuteron), the isospin of the produced charmed baryon can be controlled (Fig. 3-(b) and (c)). The spectrometer system is charge symmetric, as described in Section III B. Choosing the reaction mode (c) in Fig 3, we can measure an exotic channel, as shown in Fig. 3-(d).

To date, there has been no experimental observation of charmed baryons in the missing mass spectrum of the (π^-, D^{*-}) reaction. Only one report has given an upper limit on the cross section, ∼270 nb at an incident pion momentum (p_π) of 13 GeV/c [15]. We estimate the production cross section to be at a level of 1 nb, employing a Reggeon exchange model [16], as described in Appendix E. We have therefore improved the sensitivity by two orders of magnitude over the previous experiment. On the other hand, the reaction cross section with a positive kaon production, which is a potential source of background, is estimated to be as high as 1.8 mb at $p_\pi = 15$ GeVc [17]. The total cross section of a π^- collision with a p with strange particle production has been measured to be 3.4 mb [18]. We can reduce the background contamination by an order of 6 to 7 by identifying charmed particle production twice, namely D^{*-} and D^0 in a decay chain of $D^{*-} \to \bar{D}^0 + \pi^-$ followed by $\bar{D}^0 \to K^+\pi^-$.

Details are described in Section III B

III. EXPERIMENTAL FACILITY

A. Beam Line Configuration

1. Concept

The high-momentum (high-p) beam line was designed for the E16 experiment [19] to use a 30-GeV primary beam. The high-p beam line branches off at the SM point located at the middle point of the slope in the switch yard of the slow extraction beam line. A small fraction of the primary beam, about 10^{10} protons per spill, is delivered for E16 through the high-p beam line. Since a production target of up to 15-kW beam loss can be placed at SM, an intense pion beam can be produced through the beam line.

We have reconsidered the high-p beam line design so that high-momentum unseparated secondary beams of sufficient intensity can be made available for the present experiment. The beam line must be compatible with the use of the primary and secondary beams without major rearrangement of the beam line elements. We require the following from the high-p beam line:

- A pion beam of up to 20 GeV/c to produce excited charmed baryons for study.
- A momentum resolution of 0.1% so that a missing mass resolution at a level of 5 MeV can be achieved.
- A large acceptance of the beam line to achieve an intense pion beam of greater than 10^7 particles per second.

2. Optical Design

The beam line layout is shown in Fig. 4. It is composed of three parts, corresponding to three focal points, IF, DP and FF. In the first part, secondary beams produced at SM are collected and focused on IF. Here, we use four quadrupole magnets (Q) and one horizontal and one vertical bending magnet. The first Q magnet, which determines the solid angle of the beam line, is located 4.5 m downstream of SM. It has to be ensured that this magnet yoke does not intercept the primary beam. A vertical bending magnet has to be placed before IF in order to bend the beam down to the beam level of the hadron hall. The magnifications in the horizontal and vertical directions are set to -1.591 and -2.398 at IF. The beam size is redefined by collimators placed at IF.

In the second part, the beam is focused at DP to create a dispersive focus, where there is a strong correlation between beam momentum and beam position. We employ three

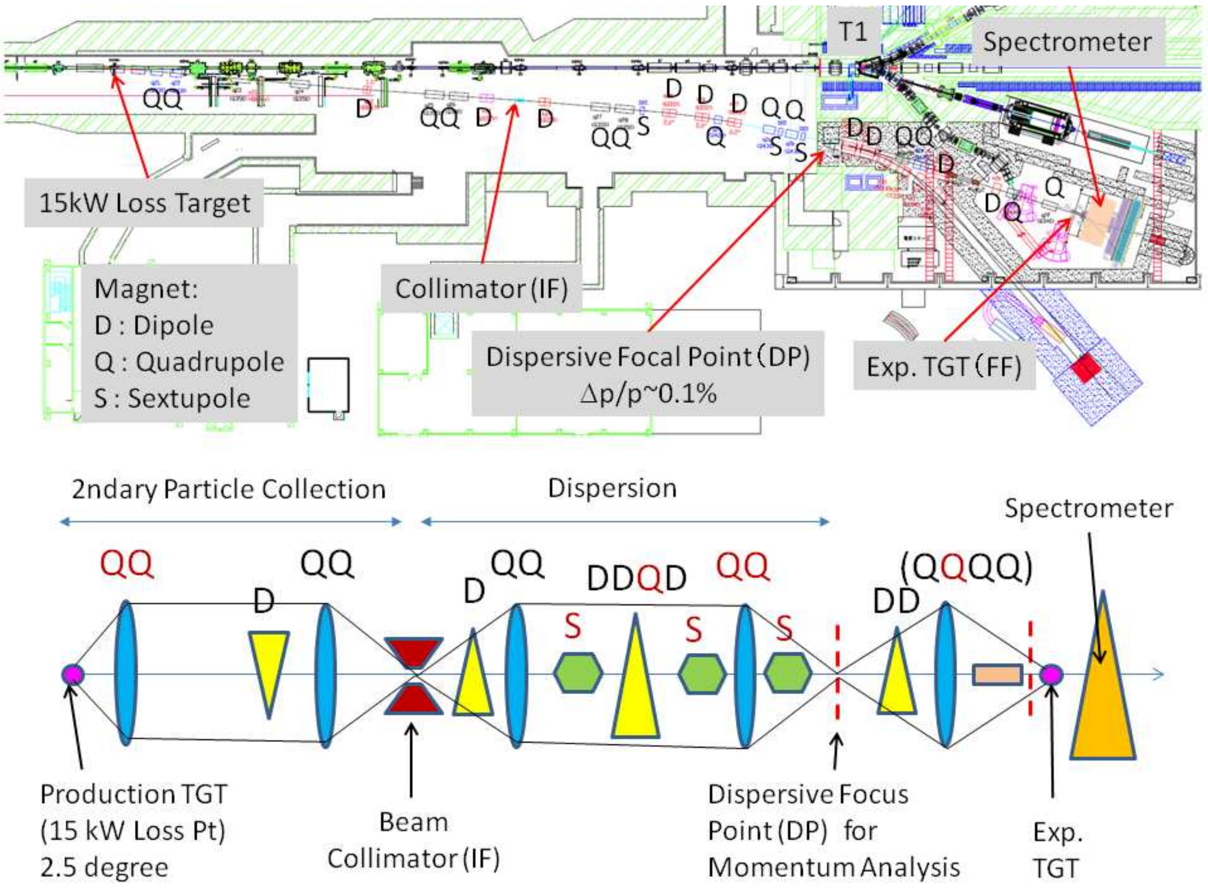

FIG. 4: Beam line layout.

bending magnets to create sufficient dispersion and four quadrupole magnets to focus the beam. The magnifications in the horizontal and vertical directions at DP are 0.664 and 4.658, respectively. The momentum dispersion is 1.031 cm/%. We employ three sextupole magnets (S) to eliminate second-order aberrations. We expect a momentum resolution of $\sim$0.1% in measuring the position of a secondary particle with a spatial resolution of 1 mm at DP. The contribution of the beam momentum resolution of 0.1% to the missing mass resolution is estimated to be about 4 MeV in the $p(\pi,\bar{D})\Lambda_c$ reaction at an incident momentum of 15 GeV/c.

In the last part, the beam is focused on FF with momentum dispersion. The magnifications of the horizontal and vertical directions at FF are -1 and -1.678, respectively. By using three bending magnets, each of which has a 6-m long pole length, and seven quadrupoles, we obtain a momentum dispersion of 1.207 cm/% at FF.

The beam envelope of the high-p beam line is calculated to the second order by TRANSPORT [20], as shown in Fig. 5. In this beam optics, the momentum resolution is estimated by the ray-tracing computer simulation code TURTLE [20]. Fig. 6 shows a strong correlation of the beam displacement with the beam momentum. When selecting the beam position in

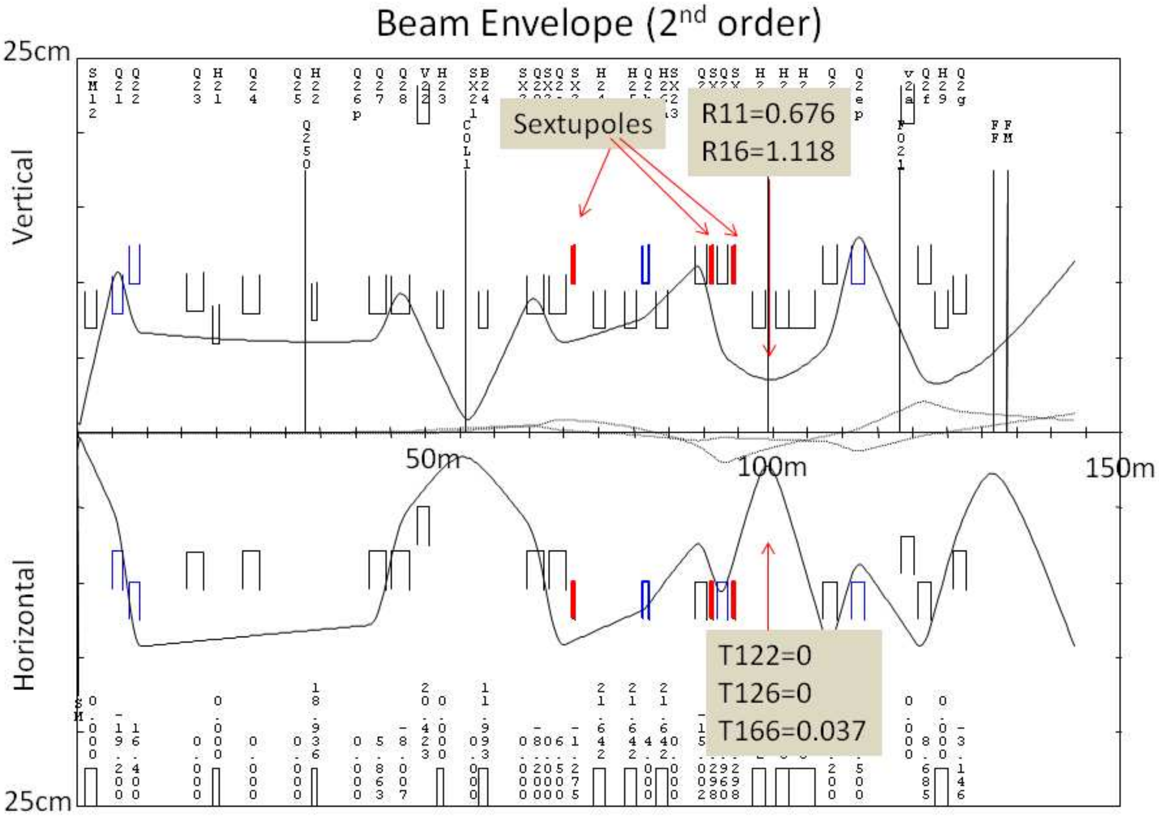

FIG. 5: Beam envelope calculated to the first-order transport matrix.

a 2-mm wide bin, the r.m.s. width of the momentum distribution in any bin is kept at a level of 0.1 %. In this simulation, the acceptance of the beam line is estimated to be about 2 msr*%. We estimate the yields of secondary particles by the Sanford–Wang formula [21]. We assume a production angle of 2.5 degrees and a 15-kW primary beam loss at a platinum target. In-flight decays through the beam line length of 132 m are taken into account. The intensity of 15-GeV/c negative pions is estimated to be $6{\times}10^7$ particles per spill (2 sec. spill, 6 sec. interval).

B. Conceptual Design of the Charmed Particle Spectrometer System

The purpose of our experiment is to measure the excited charmed baryon states in a mass region up to about 3 GeV. To reveal the properties of excited charmed baryon states, the missing mass spectroscopy method is mainly used in the experiment. The mass and width of the excited states are determined by the missing mass method. The production cross sections are measured to investigate the production mechanism. In addition, the decay products from excited baryons are measured, such as for the $Y_c^* \to Y_c + \pi$ decay, and the decay chain which decays to the known states is analyzed. From these, the spin and parity of the excited states

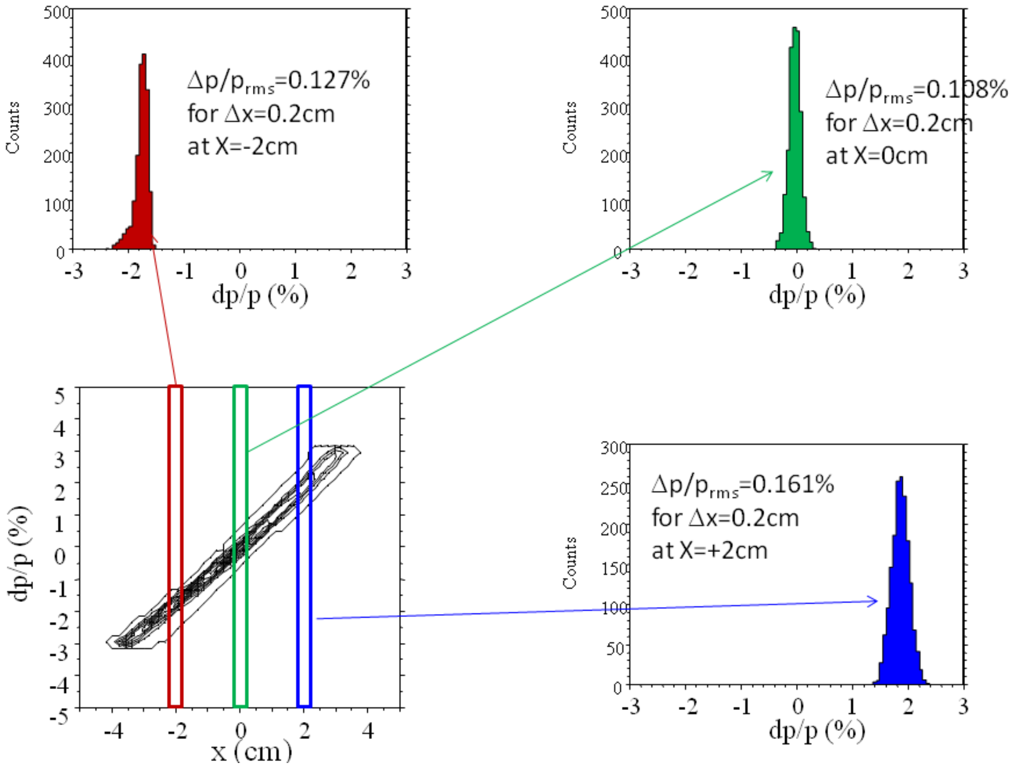

FIG. 6: Dispersive beam correlation at FF.

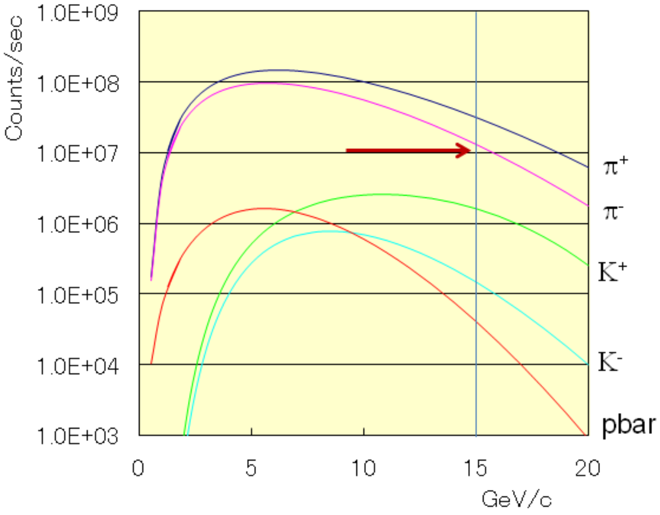

FIG. 7: Yields of secondary particles at a production angle of 2.5 degrees for a 15-kW primary beam loss at a platinum target, calculated by the Sanford–Wang formula [21]. The acceptance and total length of the beam line are 2 msr*% and 132 m, respectively.

can be determined. The excited charmed baryon states could be completely measured in the experiment.

In this study, the $\pi^- + p \to Y_c^* + \bar{D}^{*-}$ reaction is used. The $\bar{D}^{*-}$ meson decays by the $\bar{D}^{*-} \to \bar{D}^0 + \pi^-$ channel (branching ratio of 67.7%). Then, the $\bar{D}^0$ meson decays by the $\bar{D}^0 \to K^+ + \pi^-$ channel (branching ratio of 3.88%). The decay products K^+ and π^- from $\bar{D}^0$ and π^- from $\bar{D}^{*-}$ are the main particles detected by the spectrometer. The spectrometer is designed to detect the final state of the "K^+, π^-, π^-" mode. The other decay modes of the $\bar{D}^0$ meson, all of which include charged particles, can also be measured, depending on the spectrometer acceptance.

The detector configuration of the spectrometer is designed to satisfy the following experimental requirements:

- Large acceptance for $\bar{D}^{*-}$ decay particles (multi-particles measurement)
- Mass resolution as good as 5 MeV/c^2 to search for excited charmed baryons
- Particle identification (K and π) performance up to 10 GeV/c
- High-rate capability for handling the high-rate beam.

The decay products K^+ and π^- from the $\bar{D}^0$ decay have high momentum, up to 10 GeV/c for a beam momentum of 15 GeV/c. These particles are scattered in the forward direction and hence large forward detectors are installed at both the entrance and exit of the magnet. The soft π^- from $\bar{D}^{*-}$ has low momentum of less than 1 GeV/c due to the small Q-value of the $\bar{D}^{*-} \to \bar{D}^0 + \pi^-$ decay. To maintain the acceptance, it is necessary to install specific detectors to detect soft π^-. One of the known higher excited charmed baryons $\Lambda_c(2880)^+$ has a total decay width of 5.8±1.1 MeV [13]. A missing mass resolution of as good as 5 MeV is necessary to measure the higher excited region with a narrow width. This value is sufficient to measure the excited states having widths wider than $\sim$70 MeV such as $\Sigma_c(2800)$ [22]. The scattered particles have high momentum of up to 10 GeV/c. Due to the limited flight length to maintain the acceptance, the scattered particles cannot be separated by time-of-flight measurement. We plan to use the RICH counter. The production cross section is estimated to a level of 1 nb in Appendix E so it is necessary to use the intense J-PARC beam of more than 10^7 Hz. To measure the beam and scattered particles downstream of the target, detectors with high-rate capability are required. The spectrometer system was designed to satisfy these experimental requirements.

1. *Conceptual Design of the Spectrometer*

Figure 8 shows the conceptual design of the spectrometer. The FM cyclotron magnet, used in the J-PARC E16 experiment [19], will be used. The magnet has a large pole gap space and an inner space for installing inner detectors to measure soft π^- from the $\bar{D}^{*-}$ decay.

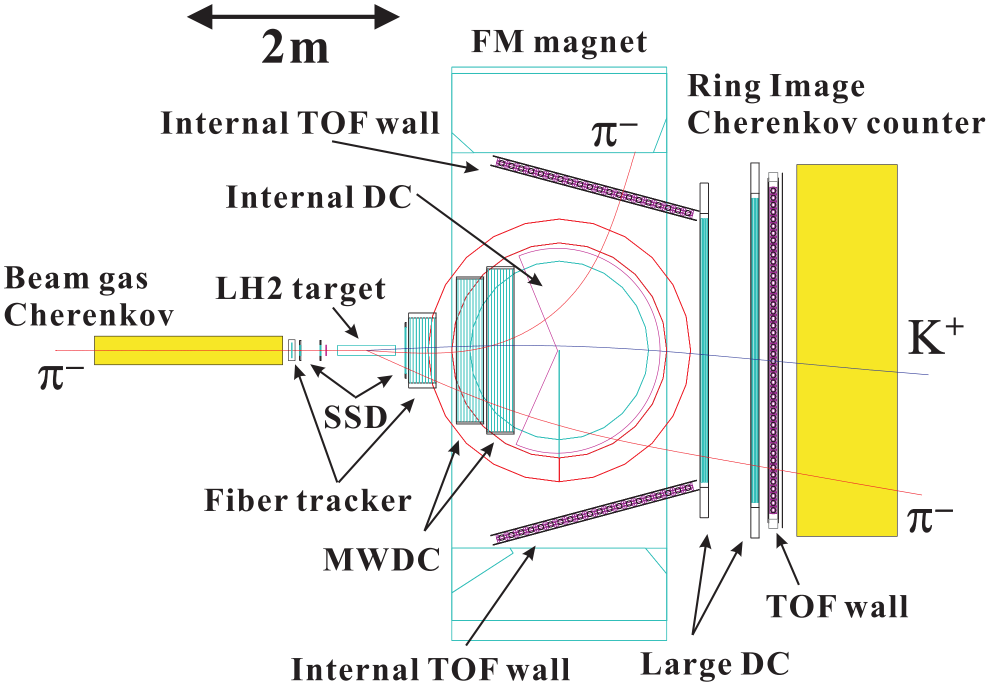

FIG. 8: Schematic view of the proposed spectrometer

These properties are suitable for a charmed baryon spectrometer with large acceptance. The FM cyclotron magnet is modified for the charmed baryon spectroscopy experiment by changing the pole pieces. The gap of the magnet pole is changed to 1 m and a maximum field strength of 1 T is used. This corresponds to a $B \times L$ value of 2.3 Tm.

To increase the yield of the excited charmed baryon states, a long liquid hydrogen target is used. The length of the target is 570 mm, which corresponds to a mass thickness of 4 g/cm^2. This mass thickness was determined to the contribution of the target energy loss straggling to the invariant mass resolution for reconstructing both $\bar{D}^0$ and $\bar{D}^{*-}$ mesons. The experimental target is placed at the entrance of the magnet. The position of the target was optimized to maximize both the acceptance and bending angle for the scattered particles. In the simulation, the scattered particles are generated isotropically inside the target along the beam direction.

The pion beams are measured by silicon strip detectors (SSD) for tracking and a fine segmented plastic scintillation counter for timing. The timing counter determines the time-zero. The horizontal size of each segment is adjusted so that it operates in a single counting rate of a few MHz. By assuming a horizontal beam size of 100 mm and expecting a counting rate of 30 MHz, the size needs to be less than 5 mm. In addition, to reject accidental events in the beam tracking, a scintillating fiber wall with a 1-mm pitch segment is installed. By gating the narrow fiber timing window of ∼1 ns and comparing the hit position on the fiber wall with the tracks measured by the SSD, accidental events from intense pion beams

(30 MHz) can be rejected. A segmented gas Čerenkov counter is installed upstream from the fiber wall. To separate the beam π^- from K^- particles with a beam momentum of 15 GeV/c, a CO_2 gas Čerenkov counter is used.

To detect K^+ and π^- from the $\bar{D}^0$ decay, tracking detectors are installed at both the entrance and exit of the magnet. The coverage of the forward tracking detectors for detecting K^+ and π^- from the $\bar{D}^0$ decay is determined from the momentum and angular distribution by simulation, assuming an isotropic angular distribution of the $\pi^- + p \to Y_c^* + \bar{D}^{*-}$ reaction in the center of mass system. The detectors at the entrance of the magnet have horizontal and vertical sizes of 400–600 mm and 200–300 mm, respectively. For the tracking devices, an SSD and a scintillating fiber tracker (1 mm pitch) are used due to the high-rate beam. The sizes of the downstream detectors are 2000–3000 mm and 1200–1500 mm in the horizontal and vertical directions, respectively. Large drift chambers with smaller drift spaces (∼10 mm) are used for the downstream tracking devices. The wires where the beam passes though are kept inactive by having no high voltage applied. Redundancy is ensured by increasing the number of tilted wire layers. The TOF wall has a similar size than the downstream tracking detectors. Large downstream detectors are needed to maintain the acceptance. A PID counter is installed downstream from the TOF wall. The details of the PID counter are described in Sec. III B–2.

Inner counters are installed inside the magnet gap. To measure the tracks of both soft π^- from the $\bar{D}^{*-}$ decay and K^+ and π^- from the $\bar{D}^0$ decay, internal tracking drift chambers of planner and cylindrical types are installed downstream of the entrance detectors. The wires where the beam pass though are kept inactive by maintaining redundancy by using sufficient tilted wire layers. The time-of-flight of soft π^- from the $\bar{D}^{*-}$ decay is measured by the internal TOF counters located at the magnet gap. By using these internal detectors, the decay particles and decay chain of higher excited Y_c^* states can also be measured, because the decay particles are scattered in the forward direction. The decay particle measurement is described in Sec. III B–8.

2. Particle Identification

The momentum of the scattered particles from the $\bar{D}^0$ decay range up to 10 GeV/c. The time difference between K^+ and π^- is estimated to be ∼60 ps for a momentum of 5 GeV/c, using a typical spectrometer flight-path length of 4 m. The conventional time-of-flight measurement cannot be used for particle identification, so timing counters such as the time-zero and the TOF counters are used to select the prompt timing of the scattered particles. On the other hand, the slow particles from the $\bar{D}^{*-}$ and Y_c^* decays can be identified using the time-of-flight information from the internal counters.

Fast scattered particles are identified using the RICH counter located downstream of the TOF wall. In the experiment, a hybrid-RICH system is planned. The hybrid-RICH system

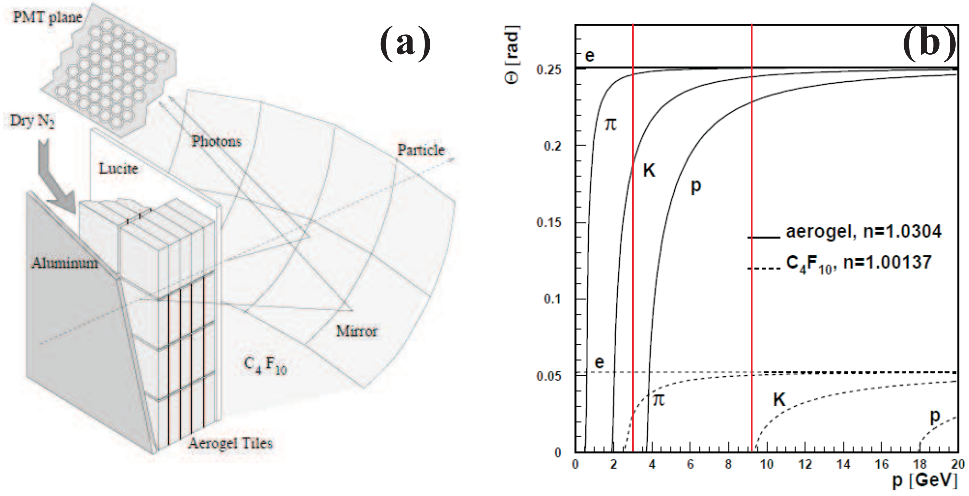

FIG. 9: Geometry and radiator configuration for the HERMES RICH (a) and the Čerenkov emission angles versus hadron momentum for the aerogel and the C_4F_{10} gas radiators (b)

was used in the HERMES experiment [23]. The HERMES RICH detector consisted of aerogel (n = 1.0304) and C_4F_{10} gas (n = 1.00137) radiators. Based on the different thresholds and the Čerenkov emission angles of these radiators, the particles (π, K, p) with momenta of 2–15 GeV/c could be separated. Figure 9 shows the geometry and radiator configuration for the HERMES RICH and the Čerenkov emission angles versus hadron momentum for the aerogel and C_4F_{10} gas radiators. For momentum less than 3 GeV/c, the aerogel is used as a threshold type Čerenkov detector for separating K and π. In the momentum range from 3 GeV/c to 9.3 GeV/c, the aerogel is used as a RICH type detector for K and p, and the C_4F_{10} gas is used as a threshold type detector for K and π. Above 9.3 GeV/c, the C_4F_{10} gas is used as a threshold type detector for K and p and as a RICH type detector for K and π. For the charmed baryon spectrometer, a similar hybrid-RICH detector will be developed.

3. High-rate and Multi-particle Tracking System

An intense π^- beam of 6.0×10^7/spill (30 MHz for a 2 sec extraction) is planned for the experiment. This beam intensity is over the limit for wire chamber operation and hence high-rate detectors are needed to handle the beam. For beam measurement, SSDs and a scintillation fiber wall are installed. An SSD (80 μm pitch and 60 mm×60 mm) has a high-rate capability of up to 10^8 Hz and that of the scintillation fiber is a few MHz per 1 mm segmentation. These capabilities are calculated assuming a 100 mm horizontal beam and expecting a total counting rate of 30 MHz.

For track measurements downstream of the target, the tracking devices at the entrance of the magnet have to be operated under a high-rate beam and high-rate scattered multi-particles. The total charged particle cross section of the $\pi^- p$ reaction measured at a beam momentum of 16 GeV/c [24]. From the cross section values in Ref [24], a multi-track rate with an averaged particle number of four tracks is estimated to be 3 M/spill under the experimental conditions (4 g/cm^2 target, 6.0×10^7/spill beam). Under this condition, both accidental tracks and wrong tracking connections between tracks obtained from the entrance and exit tracking devices are expected. To avoid incorrect tracking, a redundant tracking system is planned for tracking downstream of the target. Three kinds of tracking devices will be installed, the scintillating fiber tracker for gating the narrow timing gate, SSDs for separating the tracks with precise spatial resolution and internal MWDCs for distinguishing the particle tracks and charge by using the motion in the magnetic field of the magnet. By combining these three tracking devices, it is possible to measure the multi-particle tracks under a high-rate condition without incorrect tracking. The high-rate and multi-particle tracking system is a key device for the experiment.

4. Acceptance

The acceptance of the spectrometer system was estimated by simulation. The accepted conditions are as follows.

- Both K^+ and π^- from the $\bar{D}^0$ decay pass though all the layers of tracking devices and the TOF wall.
- Soft π^- from the $\bar{D}^{*-}$ decay pass though the entrance tracking devices, the internal tracking chambers and the internal TOF wall.

The acceptance is the ratio of the number of accepted particles and generated particles, and is shown in Fig. 10(a). The bottom figures show the momentum correlation of both generated (b) and accepted (c) particles from the $\bar{D}^0$ decay in the $\Lambda_c(2880)^+$ produced case with a beam momentum of 15 GeV/c. The horizontal and vertical axes are the acceptance and the known charmed baryon mass, respectively. The $\bar{D}^{*-}$ meson is generated by assuming an isotropic and forward ($\propto e^{-at}$) angular distribution of the $\pi^- + p \to Y_c^* + \bar{D}^{*-}$ reaction in the center of mass system. The decay angular distributions of both $\bar{D}^{*-}$ and $\bar{D}^0$ are isotropic in the center of mass system. By using the forward peak, the scattering angle of the generated $\bar{D}^{*-}$ is found to be less than 3° so that due to the large opening angle of the D^0 decay, the acceptance decreases in the higher mass region. The acceptance of the $\bar{D}^0$ decay particle detection is mainly determined by the gap of the FM cyclotron magnet. When K^+ and π^- from the $\bar{D}^0$ decay are accepted, ~90% of soft π^- from the $\bar{D}^{*-}$ decay pass are detected by the internal detectors. These soft π^-s have a momentum of 0.3–1.1 GeV/c and are scattered to a polar angle of 0°–8°. By including the decay process of K^+ and π^-s, the acceptance is decreased to ~75%. The decay factor of K^+ and soft π^- are ~0.85 and ~0.90, respectively. The absolute value of the acceptance strongly depends on

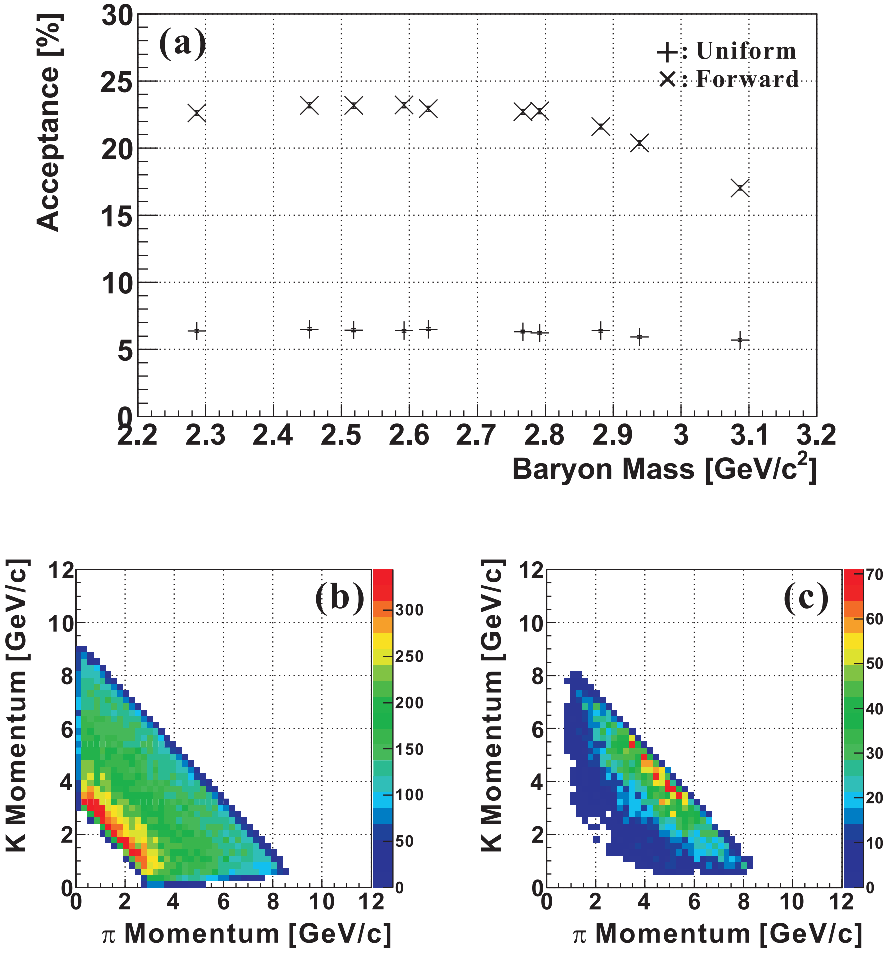

FIG. 10: (a): Acceptance for $\bar{D}^{*-}$ as a function of the missing baryon mass. $\bar{D}^{*-}$ is isotropically generated in the CM system. Momentum distributions of K^+ versus π^- from $\bar{D}^0$ generated (b) and detected (c) for $\Lambda_c(2880)^+$ production.

the angular distribution of the $\pi^- + p \rightarrow Y_c^* + \bar{D}^{*-}$ reaction. If the angular distribution of the reaction is forward peaked, the acceptance becomes a few times higher than that of the isotropic distribution.

5. Resolution

The momentum resolution, the invariant mass resolution for reconstructing the $\bar{D}^0$ and $\bar{D}^{*-}$ and the missing mass resolution are estimated by simulation. Realistic materials are input into the simulation: liquid hydrogen for the target, silicon for the SSDs, a plastic scintillator for the timing counters and the scintillation fibers, drift chamber gas (Ar:iso-C_4H_{10}) for all the chambers, and helium gas for the gap of the magnet. For tracking the position resolutions of the SSDs, fiber tracker and drift chambers are assumed to be 100 μm, 200 μm and 200 μm, respectively. A momentum resolution of 0.2% for a momentum of 5 GeV/c is achieved. The invariant mass resolutions for reconstructing $\bar{D}^0$ and $\bar{D}^{*-}$ are estimated to be 4.6 MeV and 0.71 MeV, respectively. The contributions of the target material effect to the invariant mass resolution of $\bar{D}^0$ and $\bar{D}^{*-}$ are 2.4 MeV and 0.53 MeV, respectively. The estimated invariant mass resolutions are mainly determined by the target ΔE straggling. The missing resolutions by assuming the production of the ground state (Λ_c) and the excited state ($\Lambda_c(2880)^+$) are estimated to be 9.6 MeV and 5.5 MeV, respectively. In the case of $\Lambda_c(2880)^+$ production, the contributions of the missing mass resolution is estimated from $\Delta M^2 = \Delta^2_{Beam} + \Delta^2_{Spec} + \Delta^2_{\theta} + \Delta E^2_{target}$, where the first term is the mass resolution from the momentum resolution of the beam line and the second is that of the spectrometer. The third term comes from the resolution of the scattering angle and the last term from the target ΔE straggling. The contributions of the momentum resolution of the beam line and the spectrometer including scattering angle resolution are estimated to 3.6 MeV and 3.9 MeV, respectively, where that of the target ΔE straggling is 1.5 MeV. The contribution of the momentum resolution of the spectrometer and the scattering angle is balanced to that of the beam line. The required resolutions are found to be achieved.

6. Background Event

In the experiment, the final state of the "K^+, π^-, π^-" mode is detected by the spectrometer. All reaction events which include this mode could be background of the mass spectra. There is little information about the background processes of the π^- p reaction in the momentum region of 10–20 GeV/c. The total cross section of the π^- p reaction at a beam momentum of 16 GeV/c is 25.6 mb [25]. At this momentum, the inclusive strangeness production cross section is 3.4 mb [18]. In addition, the K^0_s production with more than four charged tracks, which could include the "K^+, π^-, π^-" mode, has a cross section of 1.1 mb [26]. Therefore, a total cross section of a few mb has to be assumed to estimate the background.

The background events are estimated by simulation. To produce background events, the simulation code JAM [17] and an isotropic phase space distribution are used for comparison. The JAM (Jet AA Microscopic transport model) code is used for the background estimation of the heavy iron collision experiment. The code includes many elemental processes, such as p p and $\pi^\pm$ p. The JAM code covers the low energy range of 1–20 AGeV, which is appropriate for our simulation. For the background of the isotropic phase space distribution, a combination of particles including the "K^+, π^-, π^-" mode are randomly assigned. These particles are generated by the N-body (5–7 bodies) kinematics which follows the phase space.

Figure 11 shows the background distribution for the invariant mass of $\bar{D}^0$ and $\bar{D}^{*-}$. To reconstruct the $\bar{D}^{*-}$ mass, the $\bar{D}^0$ mass is assumed. For comparison, both the simulation

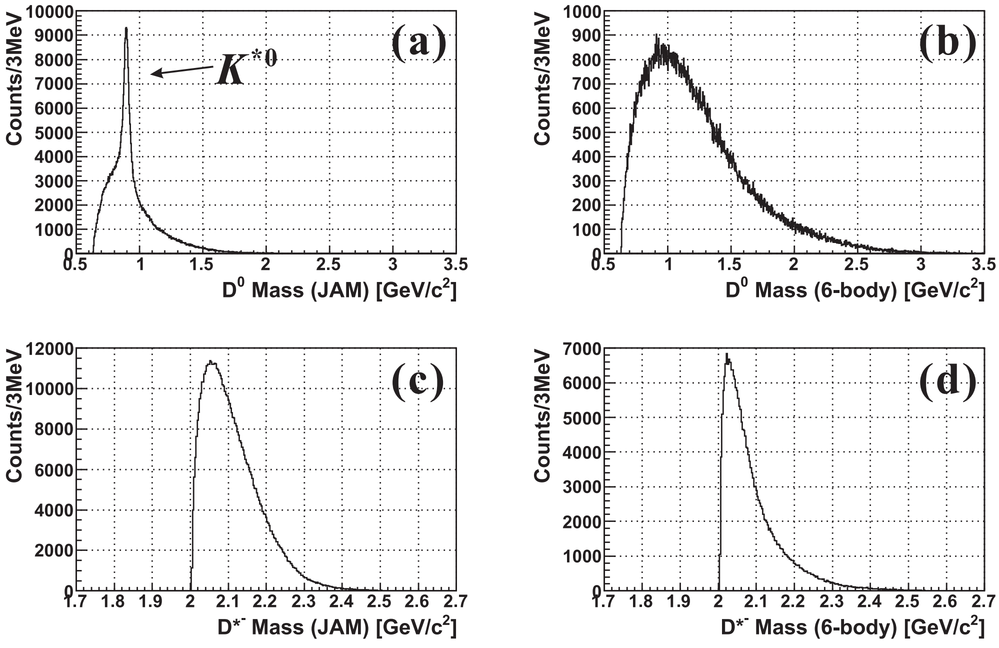

FIG. 11: Reconstructed mass spectra from K^+ and π^- ($\bar{D}^0$) (a,b) and $\bar{D}^0$ and soft π^- (c,d) in the cases of JAM (a,c) and the 6-body random background (b,d).

result by JAM and the 6-body random background are shown. Due to the processes used by JAM, a clear K^{*0} peak is observed in the spectrum. Figure 12 shows the background distribution for the missing mass spectra. By the JAM code, the average number of produced particles in an event is ∼8 so that the momentum of each particle is lower than that of the 6-body random background. The number of background events in the higher mass region is relatively larger than that of the lower region.

In the JAM code, the total cross section of the background processes, which include the "K^+, π^-, π^-" mode, is 1.8 mb. For the initial value, we employ this total cross section for the estimate. The number of background events is estimated to be 3.7×10^{11}, considering the experimental conditions (4 g/cm^2 target, 6.0×10^7/spill beam, 100 days beam time). The trigger rate is roughly estimated by the JAM simulation. By assuming a PID efficiency of 100%, the trigger rate is estimated to be 13 k/spill. This value is the accepted number of events from the JAM background. If a 2.0 sec extraction is assumed, the trigger rate becomes 6.5 kHz.

The reduction of the background is tested by a simulation. In the experiment, the invariant masses of the $\bar{D}^0$ and $\bar{D}^{*-}$ mesons are reconstructed step by step. This analysis method is called "D^* tagging". By using D^* tagging, the background events can be drastically reduced because the combinations of background events which enter the mass gate are drastically decreased. As shown in Fig. 13, by gating both the $\bar{D}^0$ and $\bar{D}^{*-}$ masses of the

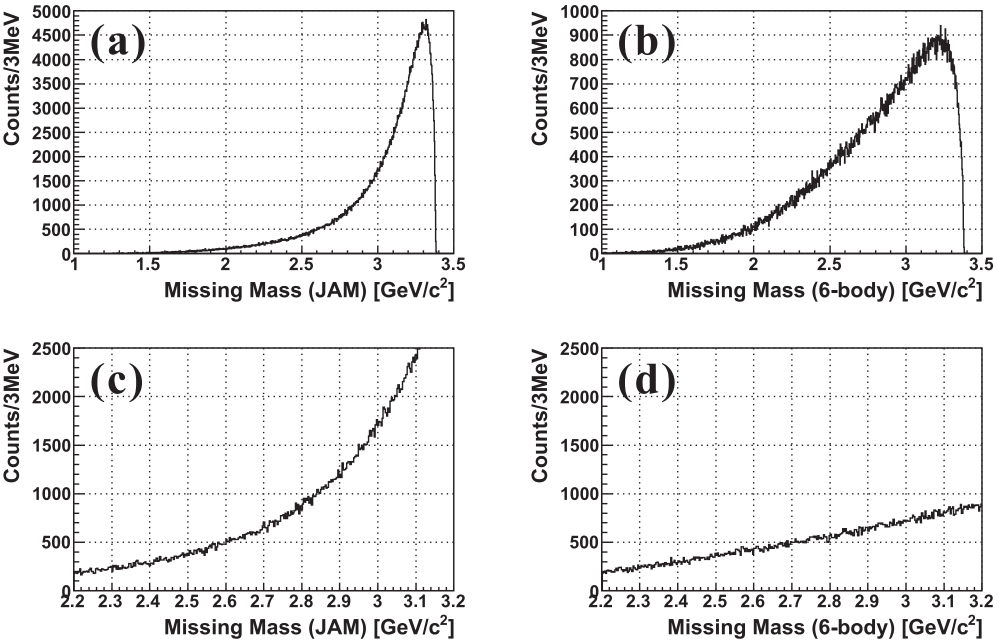

FIG. 12: Missing mass spectra for the background events. (a,c): JAM and (b,d): 6-body random background.

2.5σ region, the background reduction factor including the acceptance is 10^{-7} and 10^{-6} for JAM and the 6-body random background, respectively. A narrow mass gate for the high resolution spectrometer is also necessary for background reduction. Finally, the number of background events is reduced to 3.7×10^{4}–10^{5}.

7. Missing Mass Spectra

By assuming reduction factors of 10^{-7} and 10^{-6}, missing mass spectra with known charmed baryon resonances are generated. For the production of charmed baryon states, a cross section of 1 nb is assumed with the PDG mass and width. The events are generated by assuming an isotropic angular distribution of the $\pi^- + p \rightarrow Y_c^* + \bar{D}^{*-}$ reaction in the center of mass system. Figure 14 shows the missing mass spectra simulated with signal and background events. The background shape generated by JAM is assumed and the number of total events generated is set to be that of the reduced ones. For the higher excited region (2.65–3.10 GeV/c^2), the significance of the charmed baryon states is estimated by assuming the decay width. Figure 15 shows the significance of the total cross section of 1 nb ($\sim$1000 counts) for a reduction factor of 10^{-6}. By changing the decay width, we found that a reduction factor of less than 10^{-6} is necessary to determine the wider decay width state.

To reduce the background further, forward proton detection is applied. Protons from

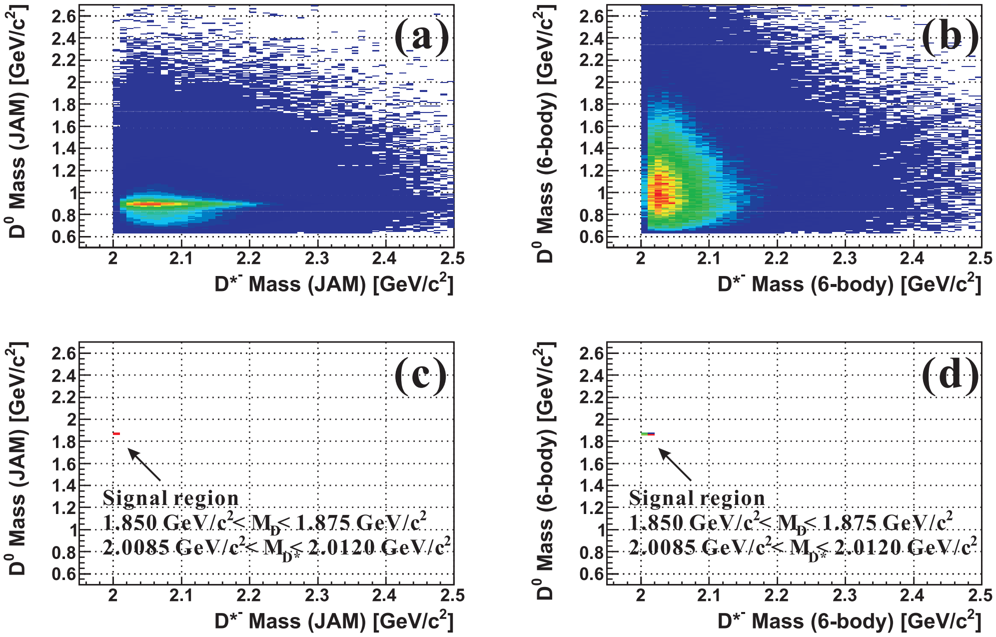

FIG. 13: Two dimensional plots of reconstructed $\bar{D}^{*-}$ and $\bar{D}^0$ masses for JAM and 6-body background events (a,b). By applying D^* tagging, only a part of the background events remain in the selected mass region (c,d).

the decay of the charmed baryon states have a high momentum due to the large momentum transfer, while protons from the background have lower momentum. The background protons are mainly produced by multi-meson production and hence the momentum transfer is smaller than that of the charmed baryon production. By detecting forward protons, the background events generated by JAM are reduced to ∼1/10. The signal from the charmed baryon states is also reduced due the proton decay breaching ratio of 50%. By optimizing the acceptance for the forward protons, the signal to noise ratio could be further improved. For a total production cross section of 1 nb, a background reduction factor of 10^{-6} is the limit for observing higher excited charmed baryon states with a wide width.

8. *Measurements of Decay Products from Excited Baryons*

From the measurement of decay products from excited baryons, such as from the $Y_c^* \to Y_c + \pi$ decay, and the analysis of the decay chain to the known states, the spin and parity of the excited states can also be determined. The excited charmed baryon produced has a large momentum in the beam direction so that the decay products of these baryons can still be detected in the forward region. Figure 16 shows the π^+ angular distribution in the center of mass system ($\cos\theta_{cm}$) from the $\Lambda_c(2940)^+ \to \Sigma_c(2455)^0 + \pi^+$ decay. The angular distribution

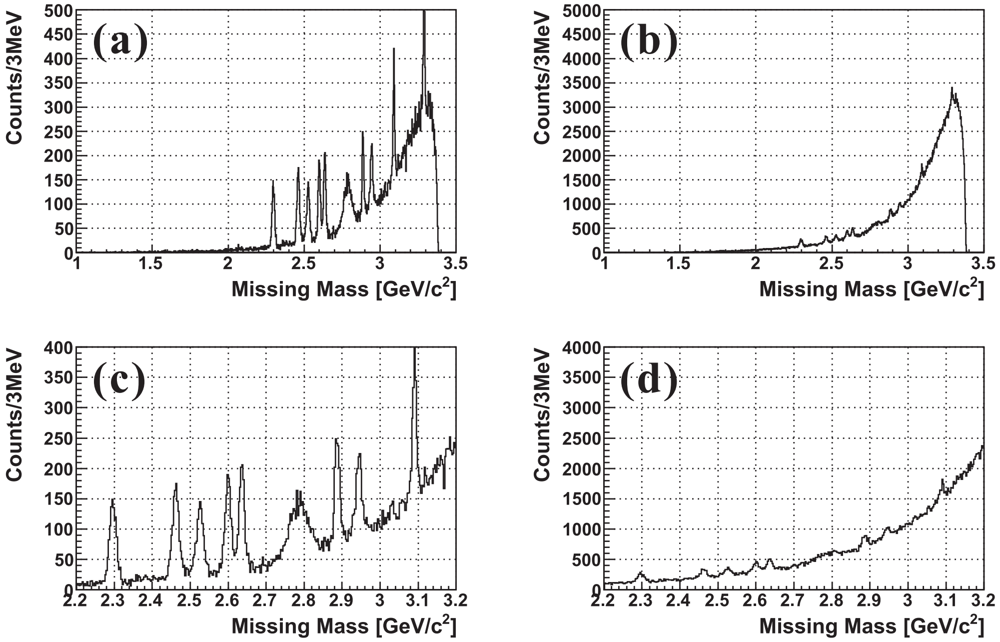

FIG. 14: Missing mass spectra simulated with signal and background events. The masses and widths of charmed baryons are assumed as reported in the PDG [3], except for the heaviest at 3.08 GeV (this is artificial). (a,c): Missing mass spectra for background events reduced to 10^{-7}. (b,d): Missing mass spectra for background events reduced to 10^{-6}.

of the $\Lambda_c(2940)^+$ decay is isotropic in the center of mass system. By detecting the forward decay particles, a large fraction of the angular distribution can be measured. The momentum vector of the excited charmed baryon state is measured by missing mass spectroscopy. By measuring the decay products, such as $\pi^{\pm}$, the mass of the daughter charmed baryon state can be determined. The mass resolution for detecting the decay modes is estimated to be 10 MeV, which is small enough to measure the daughter charmed baryon state.

9. Summary for the Spectrometer

The conceptual design of the charmed baryon spectrometer was described in this section. The spectrometer is designed for missing mass spectroscopy experiments and for the detection of the decay products of the $Y_c^* \rightarrow Y_c + \pi$ decay. Excited charmed baryon states can be completely measured systematically. The experimental apparatus includes high-rate detectors for tracking and a hybrid-RICH counter for particle identification. By using large detectors with an FM cyclotron magnet, an acceptance of 10% was achieved. The momentum resolution was estimated to be $\Delta p/p = 0.2\%$. Invariant mass resolutions of 4.6 MeV and 0.71 MeV for $\bar{D}^0$ and $\bar{D}^{*-}$ were obtained, respectively. A missing mass resolution of

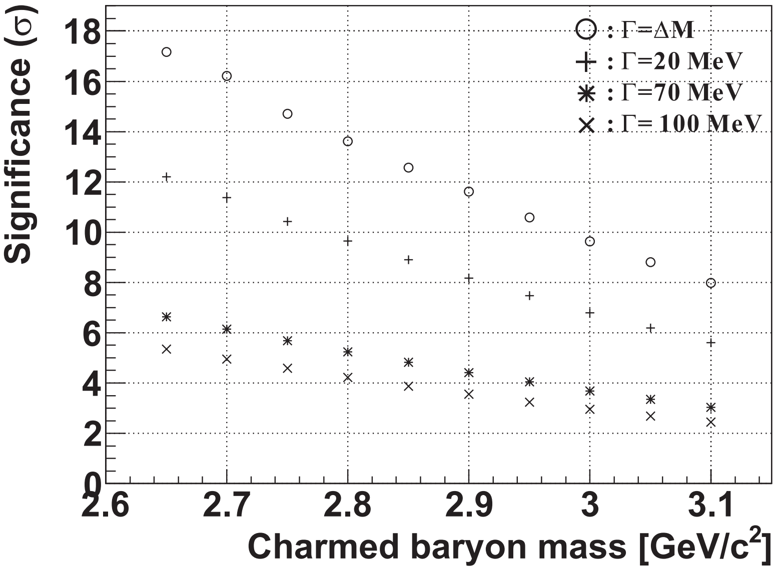

FIG. 15: Significance of the total cross section of 1 nb (∼1000 counts) for a reduction factor of 10^{-6}. The cases of the different mass windows are also shown.

5.5 MeV was achieved for $\Lambda_c(2880)^+$ production. The background events were estimated using the JAM code and an isotropic phase space distribution. The reduction factor was estimated to be less than 10^{-6} using the D^* tagging method. In the case of a total background cross section of 1.8 mb, we found that a reduction of less than 10^{-6} is necessary for the measurement of higher excited state charmed baryons with a production cross section of 1 nb. The acceptance of the decay product detection was estimated. A large fraction of the angular distribution can be measured by forward detection of the scattered particles. The mass resolution for detecting the decay modes is estimated to be about 10 MeV. It was found that the experimental requirements can be achieved.

IV. BEAM TIME REQUEST

Below, we estimate the yield of a charmed baryon. The pion beam intensity and the target thickness of hydrogen are assumed to be $6{\times}10^7$ and 4 g/cm^2, respectively. The decay branching ratios of $D^{*-} \to \bar{D}^0\pi^-$ and $\bar{D}^0 \to K^+\pi^-$, 0.67 and 0.039, respectively, should be taken into account [3]. The live time of the data acquisition is assumed to be 0.9. We estimate the tracking efficiency of the MWDCs to be 0.7. The efficiencies of pion and kaon identification are obtained to be 98% about 93% for the RICH counter of HERMES [27]. The estimated yield of a charmed baryon is then 2.3∼6.8 events/day/nb for an acceptance of 7∼21 %, as described in Section III B–4. We believe that an angular distribution with a peak

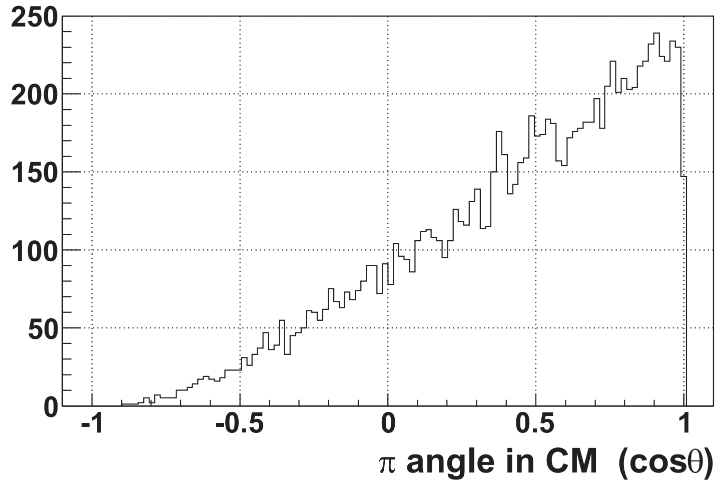

FIG. 16: π^+ angular distribution in the center of mass system ($\cos\theta_{cm}$) for the $\Lambda_c(2940)^+ \rightarrow \Sigma_c(2455)^0 + \pi^+$ decay.

at a forward angle in (π, D^{*-}) is more likely than an isotropic distribution, estimating the reaction cross sections using the equations in Appendix E. We take an average of the above estimates for the beam time request. We expect 450 events for a state having a cross section of 1 nb in a year (100 days). The first goal of the proposed experiment is to accumulate more than 1000 events so that a state with a width of 100 MeV can be observed with an improved significance, as shown in Fig. 15.

V. ORGANIZATION

The proposed experimental project is based on the Memorandum of Understanding on Research Collaboration among RCNP, KEK-IPNS, and the J-PARC Center. RCNP will share not only a portion of the facility cost but also human resources for construction and operation. The project team is expected to be in charge of collecting collaborators and conducting experimental research programs. The authors of the present proposal are to be the core members of the project team.

Once the facility is prepared, many hadron/nuclear physics experiments can be carried out [28]. For example, spectroscopic studies of nucleon and hyperon resonances via the (π, ρ) and (π, K^*) reactions, as described in Appendix F.

It should be mentioned that the present proposal has arisen from intense discussions amongst a theory group in hadron physics [29]. This project will strengthen this collaboration.

VI. COST ESTIMATION

The construction cost of the proposed experimental equipment is estimated below:

- High-p Beam line:
  KEK will be asked to make a budget request of 19.8 oku-yen for the construction of the high-p beam line to MEXT. This beam line is requested for the E16 experiment [19] for a 30-GeV primary beam. The beam line will be compatible for use as a primary or secondary beam by the addition of six quadrupole and three sextupole magnets. The additional cost for this is estimated to be about 2.1 oku-yen. The cost for the required eight power supplies is about 0.8 oku-yen if they are newly constructed. We need a primary target system of 15-kW beam loss. An indirect water cooled target system is planned, as the T1 target at a primary beam power below 50 kW, which corresponds to about 25-kW beam loss. Four bending magnets will be placed in series, with the 15-kW target being placed in the center so that a negative pion beam extraction at a production angle of 2.5 degrees is realized with the so-called beam swinger optics [30].

- Beam Line Detectors and Charm Particle Spectrometer:
  According to the design of the beam line detectors and the spectrometer system, as described in Section III, we estimate the cost to be as follows:

	amount	unit price (10^4 yen)	total price (10^4 yen)
Beam Line Detectors			
Focal Plane SFT	2	100	200
Gas Cherenkov (CO_2)	1	500	500
SSD	12	500	6000
SFT	2	100	200
Timing Counter	1	220	220
Spectrometer Detectors			
SSD	48	500	24000
SFT	9	478	4302
MWDC	4	2947	11788
Timing Counter	3	821	2463
RICH	1	20000	20000
Cabling			
34 twisted-pair cables	1545	4	6180
Coax. cables	12636	2	25272
Digitizing Electronics			
32ch TDC	773	50	38650
32ch HRTDC	139	70	9730

32ch ADC	139	70	9730

The labor cost is not included above.

APPENDIX A: QUARKS AND DIQUARKS

1. Quark Model Classification

The ingredients of the quark model are the constituent quarks which move in a single particle potential of confinement. The constituent quarks are different from the bare quarks of the QCD Lagrangian. Due to the strong interaction, the mass of the light quarks is dynamically generated: $m_s \sim m_u \sim m_d \sim 300$ MeV. Due to their rather large values and the similarity among u, d and, s quarks, quarks are treated in a non-relativistic manner, respecting spin SU(2) and flavor SU(3) symmetries. This leads to SU(6) symmetry, which is empirically very well satisfied, the basis of the constituent quark model.

We consider a classification of Qqq baryons as discussed in this proposal. In the heavy quark limit, Q behaves as a fixed center around which two light quarks move. Thus the dynamics is dictated by the two light quarks. The wave functions are then the products of spin, flavor and orbital parts. We consider here the ground state and the p-wave excited states as an example of the classification. An extension to further excited states is straightforward, though complicated.

The spin and flavor states are denoted by the dimensions of the representations. Thus spin 1/2 states are expressed by 2, spin 1 states by 3, and so on. The flavor states are 3, 6 and so on, and their conjugates are $\bar{3}$ etc. The two quark states are then classified by the irreducible decomposition of two fundamental representations of the spin and flavor group:

$$\begin{aligned} \text{spin}: \; 2 \times 2 &= 1_A + 3_S \\ \text{flavor}: \; 3 \times 3 &= \bar{3}_A + 6_S \end{aligned}$$

where the subscript shows the permutation symmetry either symmetric (S) or antisymmetric (A). Orbital states are denoted by S for the lowest s-wave state and by λ and ρ for p-wave excitations of the λ and ρ modes, respectively. Under permutation, s-wave states are symmetric, while p-wave states are antisymmetric. The λ mode corresponds to the center of mass motion of qq and ρ to the relative motion of qq. Because the color state of qq is antisymmetric $\bar{3}$ in a three quark baryon, the qq must be symmetric when spin, flavor and orbital wave functions are combined. Thus for the ground and p-wave excited states, the possible qq states are as follows:

$$\text{ground}: \quad \bar{3}\ {}^1S_0, \;\; 6\ {}^3S_1 \tag{A1}$$

$$\text{p-wave}: \quad \bar{3}\ {}^1\lambda_1, \;\; 6\ {}^3\lambda_{0,1,2}, \;\; \bar{3}\ {}^3\rho_{0,1,2}, \;\; 6\ {}^1\rho_1 \tag{A2}$$

where the notation is $D\ {}^{2S+1}L_J$, with D flavor representation, S spin value, L orbital angular momentum and J the total angular momentum. In the naive quark model, all the states of the (A1) and those of the (A2) are degenerate, separately. This is shown in the left of Fig. 17

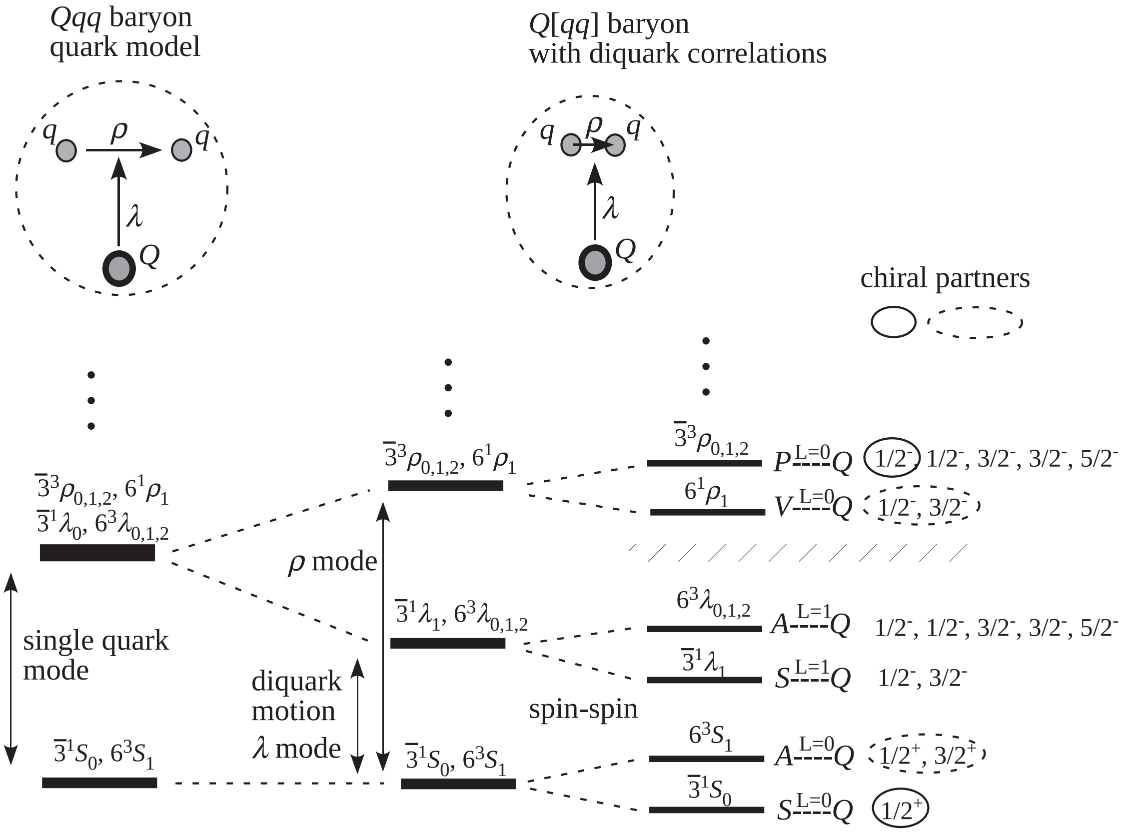

FIG. 17: Expected Qqq spectrum in a single particle picture of the quark model (left) and those with diquark correlations (middle and right). From the left to the middle, the orbital motion of λ decreases due to the collectivity of the diquark motion. From the middle to the right, spin correlations are turned on among light quarks qq. The symbols S, P, V and A are for the scalar ($^1S_0$), pseudoscalar ($^3P_0$), vector ($^3P_1$) and axial-vector ($^3S_1$) diquarks, respectively.

2. Diquarks

Diquarks can be useful for describing hadrons at low energy. A well known example was presented by Jaffe to explain the light scalar mesons, $\sigma(600)$, $\kappa(800)$, $f_0(980)$ and $a_0(980)$ [4]. The mass ordering of these mesons cannot be explained by a simple $\bar{q}q$ structure, but is naturally explained by assuming a $[qq][\bar{q}\bar{q}]$ structure, where the color anti-symmetric $\bar{3}$ scalar diquark $[qq]$ is adopted. Because of the Pauli principle, the flavor of this diquark is anti-symmetric $\bar{3}$, and so is denoted as $\bar{3}\ {}^1S_0$ in the present notation.

Table 1 summarizes the relative strengths of the color–magnetic (spin dependent) interaction

$$V_{CS} = -\sum_{ij} \frac{\alpha}{m_i m_j} \frac{\lambda^a(i)}{2} \frac{\lambda^a(j)}{2} \vec{\sigma}(i) \cdot \vec{\sigma}(j)\,. \tag{A3}$$

for all possible qq states, assuming that the orbital motion of the relative qq is the ground state. In three-quark baryons, only half of the listed states, $3\ {}^1S_0$ and $6\ {}^3S_1$, are allowed due to the Pauli principle. The other two diquarks are, however, allowed for exotic hadrons. Due to the interaction (A3), the scalar diquark $3\ ^1S_0$ is expected to be lighter than the axial-vector diquark $6\ ^3S_1$.

As Eq. (A3) shows, if the interaction depends on the inverse mass of the quarks, the diquark correlation becomes more relevant for light quark pairs, while if either or both quarks are heavy, the correlation is suppressed.

TABLE I: Matrix elements of the color–spin operator in various diquark systems.

qq	$\bar{3}\ ^1S_0$	$6\ ^3S_1$	$6\ ^1S_0$	$\bar{3}\ ^3S_1$
	$-1/2$	$+1/6$	$+1/4$	$-1/12$

It is a general feature that correlations resolve degenerate spectra in many-body systems. An example is shown in Fig. 18 for the nuclear levels expected in a simple harmonic oscillator model, compared to more realistic cases where the degenerate levels are resolved as more correlations are turned on.

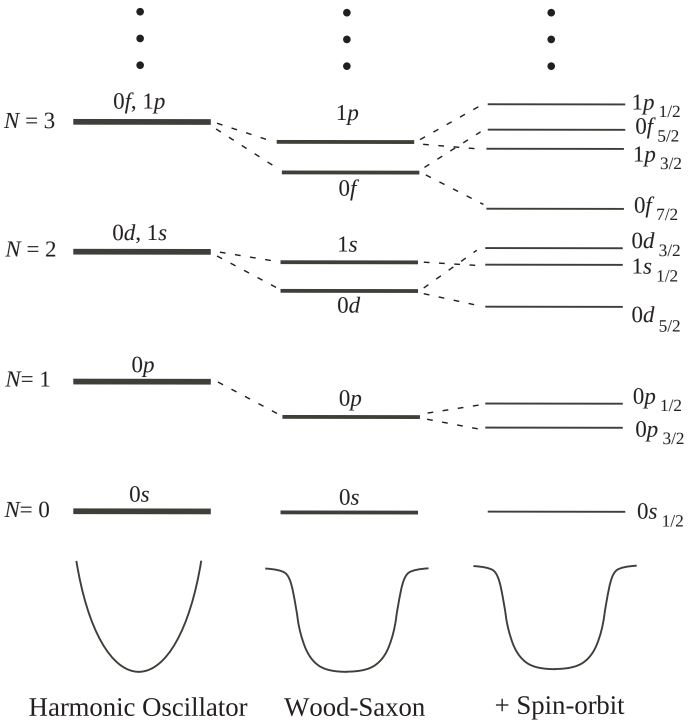

FIG. 18: Nuclear levels expected in three different potentials and the qualitative pattern resolving the degeneracy when correlations are introduced.

3. Chiral Partners

Chiral symmetry is a fundamental symmetry of QCD, and is relevant for light flavor quarks. In the present world, it is spontaneously broken and is considered to be responsible for the mass generation of light flavor hadrons. It is responsible for the masses of the constituent quarks.

The chiral symmetry transformations are

$$q \to \exp(i\gamma_5 \theta t) \tag{A4}$$

where θ is a set of transformation parameters and t is the generator of the light flavor transformations. The product θt is understood to be an inner product over the components of the adjoint representations of the flavor group.

In a relativistic construction, five kinds of Lorentz bilinear forms of diquarks are possible: $\tilde{q}q$, $\tilde{q}\gamma_5 q$, $\tilde{q}\gamma_\mu q$, $\tilde{q}\gamma_\mu\gamma_5 q$ and $\tilde{q}\sigma_{\mu\nu}q$. Here $\tilde{q} = q^T i\gamma_0\gamma_2\gamma_5$, which transforms as $\bar{q}$ under the Lorentz transformation. The bilinear forms are related by the chiral symmetry transformations (A4):

$$\tilde{q}q \leftrightarrow \tilde{q}\gamma_5 q, \tag{A5}$$

$$\tilde{q}\gamma_\mu q \leftrightarrow \tilde{q}\gamma_\mu\gamma_5 q. \tag{A6}$$

The states which transform under chiral symmetry transformations are called chiral partners. In the non-relativistic notation, there are correspondences

$$\tilde{q}q \to {}^1S_0(S), \quad \tilde{q}\gamma_\mu q \to {}^3P_1(V), \quad \tilde{q}\gamma_\mu\gamma_5 q \to {}^3S_1(A), \quad \tilde{q}\gamma_5 q \to {}^3P_0(P)\,. \tag{A7}$$

Here, the shorthand notations S, V, A, P are also used. By combining them with another quark, we can form chiral partner baryons. They are denoted by solid and dashed circles in Fig. 17.

As an empirical fact, chiral partners have a mass difference about half a GeV. This seems universal by choosing possible candidates of chiral partners in light flavor hadrons, as shown in Fig. 19. In the quark model, P and V diquarks require an internal p-wave excitation. Whether such excited diquarks survive in a hadron structure is an important question.

APPENDIX B: THRESHOLD EFFECTS AND HADRON DYNAMICS

1. Opening of Hadron Thresholds

Excited baryons are strongly renormalized by the dynamics of ground state hadrons. The opening of hadron thresholds primarily gives a decay width to excited states. Also, multi-hadrons can become constituents of excited states as hadronic molecules, if the correlations among hadrons are sufficiently strong. Hadronic correlations are primarily driven by the

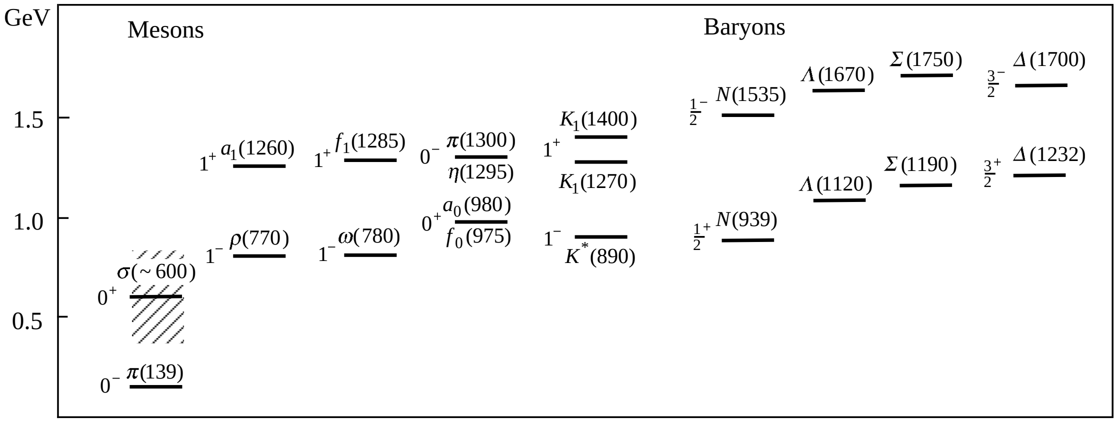

FIG. 19: Expected chiral partners of hadrons with opposite parities.

long-range dynamics among hadrons, in contrast to the short range quark–gluon dynamics in the confinement scale. An understanding of the interaction among hadrons is thus important to generate exotic hadrons and multi-quark states. These features are also discussed actively for the charmonium sector, where many findings have been recently accumulated above the open charm $D\bar{D}$ threshold [31]. In the following, we discuss various issues which can be studied in charmed baryon spectroscopy.

2. Comparison of Charm with Strangeness

To see the importance of threshold effects in excited baryon spectroscopy, let us compare the threshold energies and masses of excited hadrons in the strangeness $S = -1$ and charm $C = +1$ sectors (Fig. 20). As seen in the figure, the level ordering of the excited states of uds hadrons (Λ, Σ) is the same as that of udc hadrons (Λ_c, Σ_c). However, their energies relative to the two-body thresholds are quite different. To understand these features, let us consider the symmetries of QCD. In the massless limit $m_q \to 0$, hadrons are constrained by chiral symmetry, and in the limit $m_q \to \infty$, heavy quark symmetry becomes manifest [32]. Although these are both approximate symmetries for the charm and strange sectors, the remnant of the idealized limit can be found in the observed pattern of the spectrum.

For instance, it is instructive to compare the mass difference of the $1/2^+$ and $3/2^+$ states of Σ and Σ_c:

$$M_{\Sigma,3/2^+} - M_{\Sigma,1/2^+} \sim 192 \text{ MeV} \gg M_{\Sigma_c,3/2^+} - M_{\Sigma_c,1/2^+} \sim 65 \text{ MeV} \tag{B1}$$

This mass difference stems from the spin–spin force, which is suppressed when the quark mass is large, as a consequence of the heavy quark symmetry. Because of the reduction of the mass difference, the ground state of Σ_c lies above the $\pi\Lambda_c$ threshold. At the same time, the threshold energy of $\pi\Sigma_c$ appears higher than the $3/2^+$ state. As a consequence, the ground state of Σ_c can decay *via* a strong interaction, which is forbidden in the strangeness

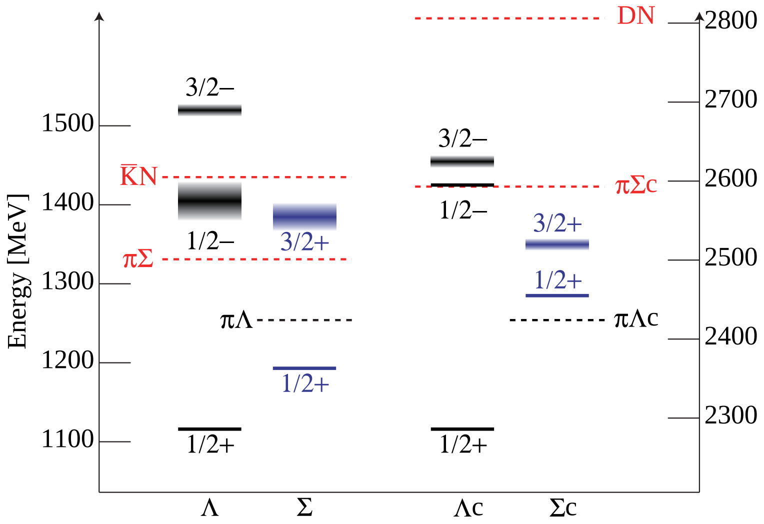

FIG. 20: Comparison of the threshold and excited state energies of the strangeness $S = -1$ and charm $C = +1$ sectors.

sector. In addition, the excited state of $3/2^+$ Σ_c cannot decay into the $\pi\Sigma_c$ channel, which is allowed in the strangeness sector. Thus, it is possible to study the effect of opening the new threshold through a comparison of Σ and Σ_c states.

Another example can be seen in the negative parity excited states of Λ (Λ_c). These states can couple to the $\pi\Sigma$ and $\bar{K}N$ channels ($\pi\Sigma_c$ and DN channels). If we compare the threshold energy differences of the $\bar{K}N$-$\pi\Sigma$ system and the DN-$\pi\Sigma_c$ system, we find

$$E_{\bar{K}N} - E_{\pi\Sigma} \sim 104 \text{ MeV} \ll E_{DN} - E_{\pi\Sigma_c} \sim 213 \text{ MeV} \qquad \text{(B2)}$$

This can be understood by chiral symmetry. π and $\bar{K}$ can be regarded as Nambu–Goldstone (NG) bosons, while the D meson cannot be, since a charm quark is too heavy to be a chiral fermion. The NG boson nature of $\bar{K}$ reduces its mass from the naively expected value in the constituent quark model. Thus, the mass difference between $\bar{K}$ and D should be much larger than the mass difference between Σ and Σ_c, which leads to the threshold energy difference in Eq. (B2). Because of the change of the threshold energies, the $3/2^-$ state of Λ_c is found below the DN threshold, and the $1/2^-$ state comes close to the $\pi\Sigma_c$ threshold.

In this way, the pattern of the threshold energies in the charm sector is different from the strangeness sector. Although the quark mass in QCD is not an adjustable parameter, the comparison of the charm and strangeness sectors enables us to extract information on the threshold effects in the structure of excited hadrons.

APPENDIX C: CHARMED MOLECULES

In this section we consider hadronic molecules containing heavy quarks as candidates of exotic hadrons. Two examples are discussed; one is the exotic baryon formed by $\bar{D}N$ [33, 34]

and the other is the dibaryon formed by $\Lambda_c N$ [37]. A common feature of these states is that the main interaction of the two hadrons is dominated by one-pion exchange. The couplings such as $\bar{D}^*\bar{D}\pi$ and $\Sigma_c\Lambda_c\pi$ are responsible for the interaction. Note that the $\bar{D}N$ system is truly exotic and requires minimally five quarks. We may be able to consider a DN system, but it requires couplings to genuine quark states such as *cud*, where more theoretical study is needed.

In the heavy quark sector, molecular states are more likely to be formed for two reasons. One is that the kinetic energy is suppressed because of a larger reduced mass. The other is that the spin degeneracy of heavy hadrons creates significant coupled channel effects. In fact, $\bar{D}^*$ and $\bar{D}$ are degenerate spin multiplets in the heavy quark limit, as are $\Sigma_c(1/2^+)$ and $\Sigma_c^*(3/2^+)$. Therefore, coupled channel effects of $\bar{D}^*N$ in the $\bar{D}N$ system, and of $\Sigma_c(1/2^+)N$ and $\Sigma_c^*(3/2^+)N$ in $\Lambda_c N$ is a driving force for the creation of bound and resonance states.

For the $\bar{D}N$ systems, the interaction was constructed by using the D^* decay into $D\pi$ as well as the well-controlled πNN coupling [34]. The results for the coupled channel analysis for the $\bar{D}N$ and BN systems are shown in Fig. 21, where an analysis was made for both the charm and bottom systems. There are several bound and resonant states with similar patterns in two flavor systems. As anticipated, bottom systems have more strongly bound and low lying resonant states due to there being more attractions.

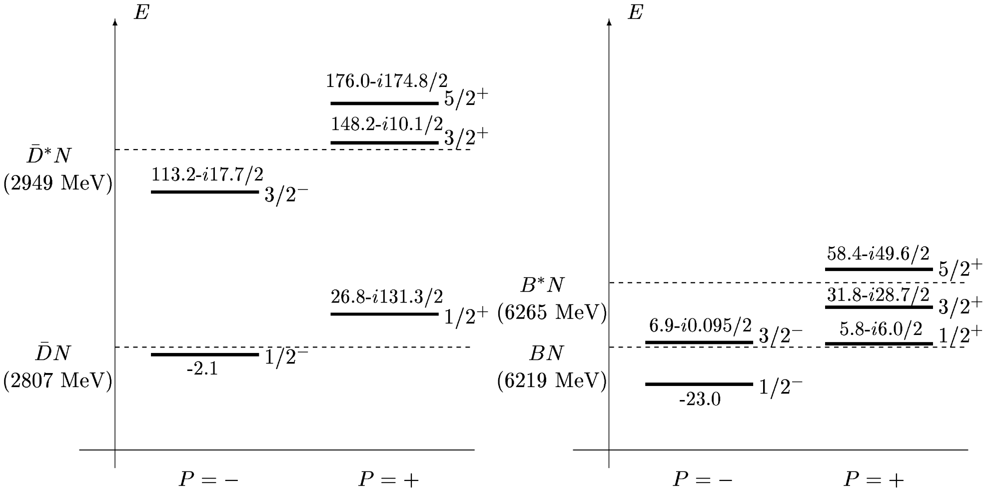

FIG. 21: Low lying bound and resonant states of exotic $\bar{D}N$ and BN systems.

For the $\Lambda_c N$ systems, the interaction between a charmed baryon and a nucleon was first studied in Ref. [35], where the authors employed a meson-exchange potential approach. Further studies carried out by Bando and Nagata [36] found that both Λ_c- and Λ_b-nuclear bound states may exist for $A \geq 4$, while no two-body bound state was found. On the other hand, recent studies [37] with modern effective theory with chiral symmetry and heavy-quark symmetry have shown that it is possible to have $\Lambda_c N$ and also $\Lambda_c\Lambda_c$ bound states.

The results show significant mixings of Σ_c and Σ_c^* baryons in the wave functions (Fig. 22), for the $J^P = 0^+$ ($\Lambda_c N(^1S_0)$, $\Sigma_c N(^1S_0)$, $\Sigma_c^* N(^5D_0)$ channels) bound state of the binding energy 6.16 MeV (left) , and the $J^P = 1^+$ ($\Lambda_c N(^3S_1)$, $\Sigma_c N(^3S_1)$, $\Sigma_c^* N(^3S_1)$, $\Lambda_c N(^3D_1)$, $\Sigma_c N(^3D_1)$, $\Sigma_c^* N(^3D_1)$, $\Sigma_c^* N(^5D_1)$) bound state of 7.52 MeV (right). The strong D-wave mixings are due to the tensor force in the one-pion exchange interaction. The same mixing phenomenon is also found in $\bar{D}N$ systems [34].

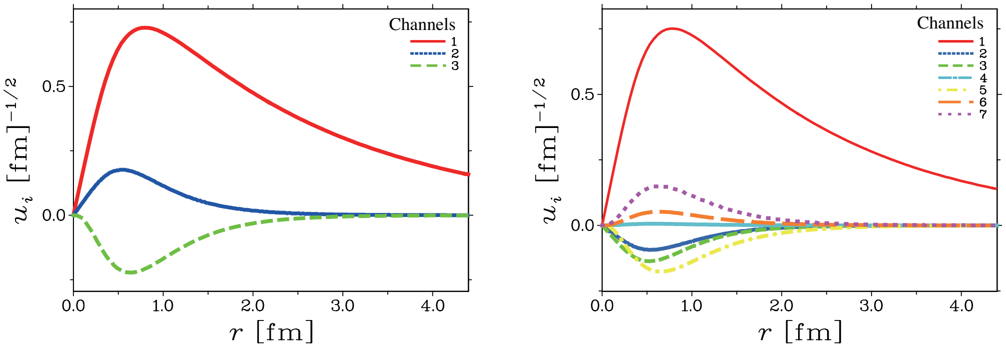

FIG. 22: Radial wave functions of various coupled channels of charmed dibaryons.

APPENDIX D: ROPER-LIKE STATE OF A CHARMED BARYON

In naive constituent quark models, the orbital angular momentum of constituent quarks can be excited with less energy than the nodal excitation. Consequently, the first excited state of a baryon is expected to have a negative parity. This expectation is, however, not realized in the actual spectrum of light-quark baryons: the first excited state, called the Roper resonance, has a positive parity, while a negative parity N^* appears in the second excited state. This "inverse phenomenon" in the N^* spectrum, is a long standing problem of hadron spectroscopy (the "Roper problem").

Several attempts have been made to resolve the Roper problem based on static hadron models, but none of them have succeeded in providing a satisfactory answer to the problem. While other qualitative features of the low-lying N^* spectrum can be understood reasonably well in the constituent quark picture, the Roper problem raises serious question of how well the constituent quarks can be used as dynamical degrees of freedom.

Recent dynamical coupled-channels analyses of meson production reactions have revealed that the hadron dynamics may produce sizable mass shifts of a few hundred MeV for the N^* energy levels obtained from the constituent quark models [38]. This suggests that the Roper problem in the N^* spectrum can be naturally explained by taking into account the hadron dynamics. The large width of the N^*, however, implies that the dispersive effect completely mixes up the naive picture of the constituent quark models. Therefore, it is difficult to identify the essential degrees of freedom to describe the baryon properties, for a study of only the light-quark baryons. On the other hand, the widths of heavy baryons are very small (about a few MeV) compared with the light-quark baryons. Thus “contamination” from reaction dynamics is expected to be greatly suppressed for the heavy baryon spectrum. The heavy baryons are therefore an ideal subject for examining whether the constituent quark picture of baryons is justified and for clarifying many questions which cannot be answered from the light-quark baryons.

The spectrum of the Qqq baryons is shown in Fig. 23. We can see that a few low-lying states appear in the simple picture, though their spin-parity is not measured. Let us assume that the heavy baryons consist of a heavy quark Q and a “diquark” (baryon number 2/3 system) with a spin-parity S^P and relative orbital angular momentum L. In this picture, the ground states Λ_c, Λ_b and Ξ_c have $S^P = 0^+$ and $L = 0$. The first and second excited positive parity states with $J^P = 1/2^+$ and $3/2^+$ (Σ_c, Σ_b and excited states of Ξ_c) can be interpreted as baryons consisting of a diquark with $S^P = 1^+$ and $L = 0$. Then, the next pair of excited states with negative parity ($J^P = 1/2^-$, $3/2^-$) can be assigned as the first orbital excited states with $L = 1$. Their excitation energies are almost the same for Λ_c and Ξ_c. Within this na?ve ?ark–diquark picture, the Roper states are assigned as the first nodal excitations of the diquark with $S^P = 0^+$ and are expected to appear with 400–700 MeV of the excitation energy for Λ_c. Therefore, the most crucial and urgent test of the constituent quark picture is an experimental identification of this correspondent of the Roper resonance in the heavy baryon sector. A precise determination of the excitation energy is also important because the nodal excitation energies purely reflect the dynamics of the underlying theory, QCD.

In the excitation energy region between 400 and 700 MeV, many baryon states may still be unobserved, in addition to the Roper resonance. There is also a possibility that heavy baryons containing negative-parity diquarks ($S^P = 0^-$, 1^-) with $L = 0$ could be found in the same energy region as the Roper-like state. At present, three baryons have been observed for the Λ_c and Σ_c excited states, as plotted in Fig. 23, while the spin and parity of only one of the three states ($5/2^+$) have been determined from experiment.

In conclusion, the experimental identification of the spectrum and spin-parity quantum numbers for the Λ_c and Σ_c excited states up to 700 MeV excitation energy will be very important for establishing a solid picture of baryons.

APPENDIX E: $p(\pi, D^{*-})X$ REACTION CROSS SECTION

To estimate the cross section of a charmed baryon (Y_c) in the $p(\pi, D^{*-})Y_c$ reaction, we employ a Reggeon exchange model based on the quark gluon string model [16]. A cross section ($\sigma(s)$) is expressed as a function of the Mandelstam variable, s:

$$\sigma(s) = C \int_{t_0}^{t_1} dt \left[\frac{1}{64\pi s (p_m^{cm})^2} g_1^2 g_2^2 |F(t)|^2 |s/s_0|^{2\alpha(t)} \right], \tag{E1}$$

$$|F(t)|^2 = \exp(2R^2 t), \tag{E2}$$

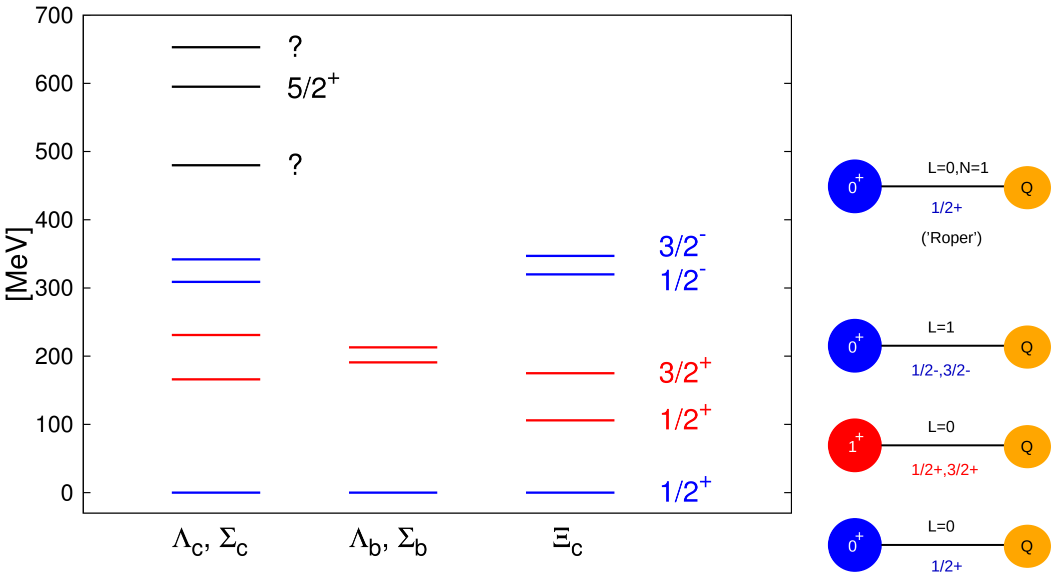

FIG. 23:

$$s_0 = (m_M + m_B)^2, \tag{E3}$$

where α is a Regge trajectory of an exchanged Reggeon in a binary reaction (Fig. 24-right), taking a non-linear Regge trajectory as a function of the Mandelstam variable t into account [39–41]. The parameter R^2 represents a slope parameter, by which the form factor ($F(t)$) of the t-channel reaction is characterized. The parameters g_1 and g_2 are coupling constants at the reaction vertex to the Reggeon. The scale parameter s_0 is taken to be the threshold energy of a binary reaction, thus m_M and m_B are the masses of scattered particles. We demonstrate that this formula reproduces the energy dependences of various binary reactions. Fig. 24-left shows measured cross sections of strange meson and baryon production in a pion collision with a proton. A solid line is calculated for $R^2 = 2.13$ (GeV/c)^2, $g_1 = 5.8$, $g_2 = 4.5$ as adopted in Ref. [39]. For $C = 0.5$, the line fits the data for the (π^-, K^0) reaction fairly well.

We next estimate cross sections of the $p(\pi, D^{*-})Y_c$ reactions as a function of incident pion beam momentum, as shown in Fig. 25-left. We use α for the D and $D*$ Reggeons shown in Ref. [41]. We find that the cross section for the ground state Λ_c has a peak at around $p_\pi = 15$ GeV/c but that for the excited state $\Lambda_c(2880)$ is greater than 25 GeV/c. On the other hand, the pion beam intensity decreases as the momentum increases. Fig. 25-left shows a figure of merit, taking the product of the intensity and the cross section. According to this figure, the momentum dependence becomes flat at around 20 GeV/c for highly excited states. The beam momentum should be chosen to be between 15 and 20 GeV/c in an experiment.

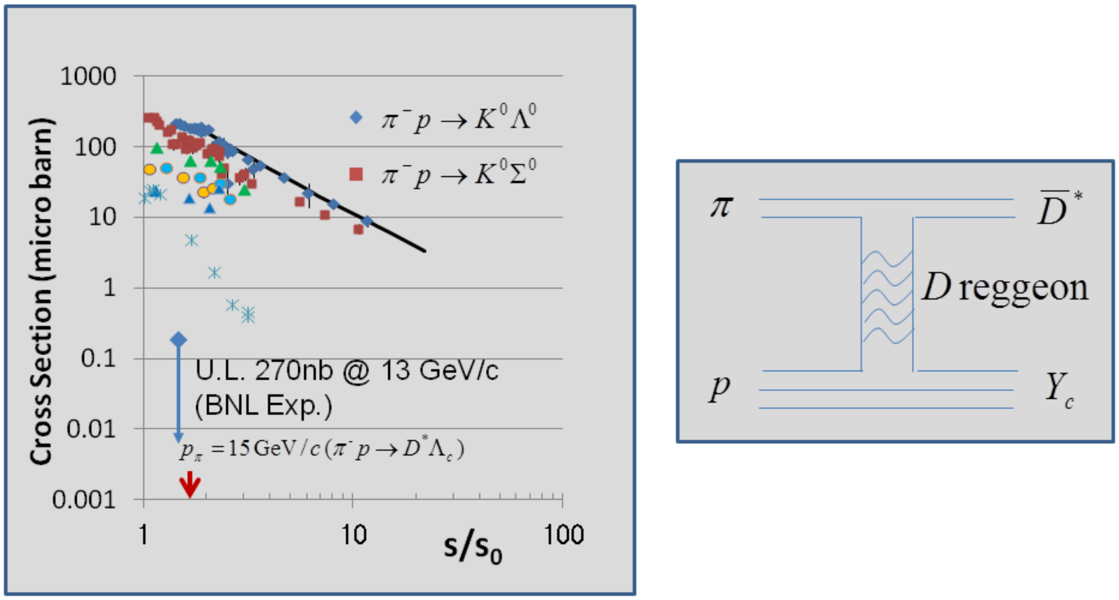

FIG. 24: Various binary reactions measured in the strange quark sector. The solid line calculated by the formula fits the energy dependence of the (π^-, K^0) reaction

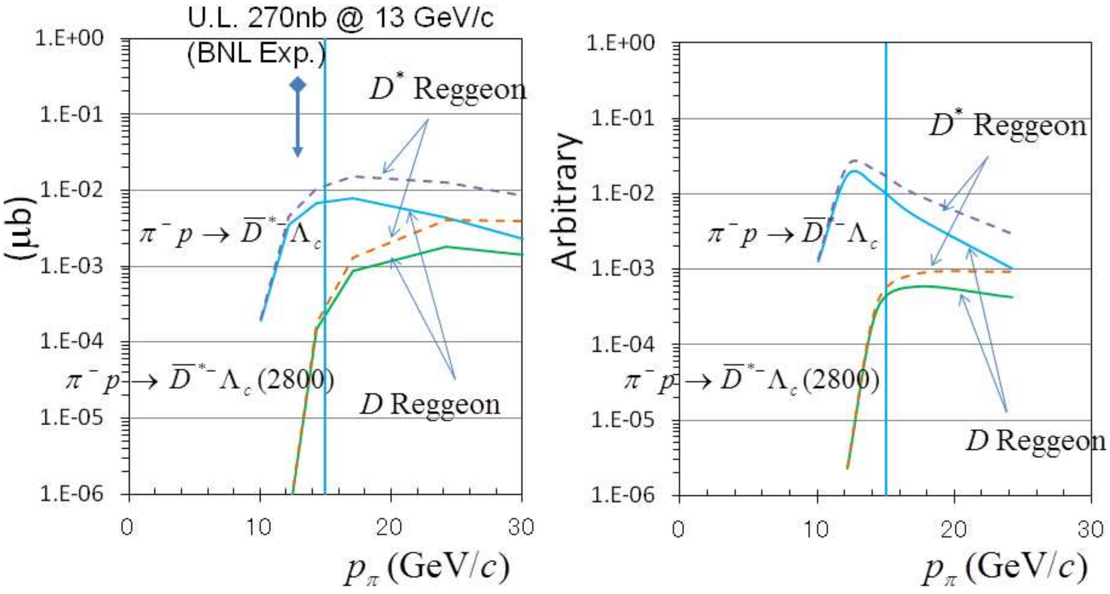

FIG. 25: Calculated cross sections for Λ_c and $\Lambda_c(2880)$ production in (π^-, D^{*-}) reactions.

APPENDIX F: AXIAL FORM FACTOR MEASUREMENT

An experimental setup for charmed baryon spectroscopy can also be used for light flavor baryons. We plan to also measure the axial vector transition form factor from nucleon to light flavor baryon resonance. The hadron form factors describe the spatial distributions of charge and current inside the hadron, and thus are intimately related to its internal structure. The fundamental understanding of the hadron form factors in terms of QCD gives the confinement mechanism, and is one of the unanswered problems in nuclear physics. To date, the electromagnetic structures (vector response) of baryons have been measured using electron scattering. We will determine the axial vector transition form factor, which corresponds to the current source of the coupling to pions and kaons, by using virtual pions and kaons. The virtual pions and kaons are realized by detecting the extremely forward produced vector mesons ρ and K^* at the high momentum secondary beamline at J-PARC. The (π, ρ) and (π, K^*) reactions for a proton are thought to give virtual pions and kaons. The axial vector form factor can be obtained from the cross sections as a function of the space-like invariant momentum transfer Q^2.

1. Form Factors

Historically, the electromagnetic form factors of the proton have been measured by using elastic electron–proton scattering, and those of the neutron have been extracted from elastic electron–deuteron scattering [42]. The elastic electric and magnetic form factors characterize the distributions of charge and magnetization in a nucleon as a function of spatial resolving power. The nucleon form factors are the matrix elements of the electromagnetic current $J_\mu = \overline{\psi}\gamma_\mu\psi$ between the initial nucleon with a momentum p and a spin four vector s and the final nucleon with p' and s', and are described as

$$\langle N(p', s')|J_\mu|N(p, s)\rangle = \overline{u}(p', s')\left[\gamma_\mu F_1(Q^2) + \frac{i\sigma_{\mu\nu}q^\nu}{2m}F_2(Q^2)\right]u(p, s) \tag{F1}$$

where m denotes the nucleon mass, q stands for the momentum transferred to the nucleon $p - p'$ and $Q^2 = -q^2$. The electric and magnetic form factors are defined in terms of F_1 and F_2 as

$$\begin{cases} G_E(Q^2) = F_1(Q^2) - \dfrac{Q^2}{4m^2}F_2(Q^2) \\ G_M(Q^2) = F_1(Q^2) + F_2(Q^2) \end{cases} \tag{F2}$$

These form factors are interpreted as Fourier transforms of the nucleon charge and magnetization densities. The elastic form factors at low Q^2 are known to approximately follow a dipole form:

$$G_D(Q^2) \propto \frac{1}{\left(1 + \dfrac{Q^2}{0.71\mathrm{GeV}^2}\right)^2}. \tag{F3}$$

This behavior can be explained by a vector meson dominance model in which the virtual photon couples to the nucleon after the fluctuation from the virtual photon into a virtual vector meson. Figure 26 shows G_E and G_M divided by G_D as a function of Q^2 for a proton obtained by the Rosenbluth cross section method. Figure 27 shows those for the neutron obtained in double-polarization experiments. The deviations from the dipole form is important at larger Q^2. Different charge and magnetization distributions are suggested for the proton [43–45].

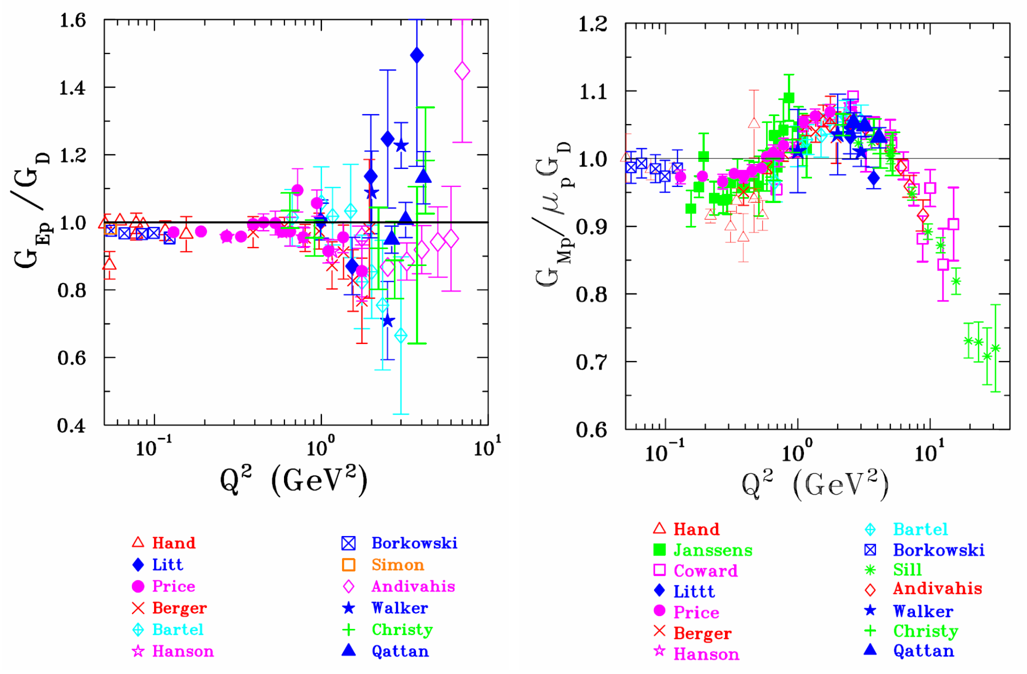

FIG. 26: Data for the proton G_E and G_M obtained by the Resenbluth cross section method [46].

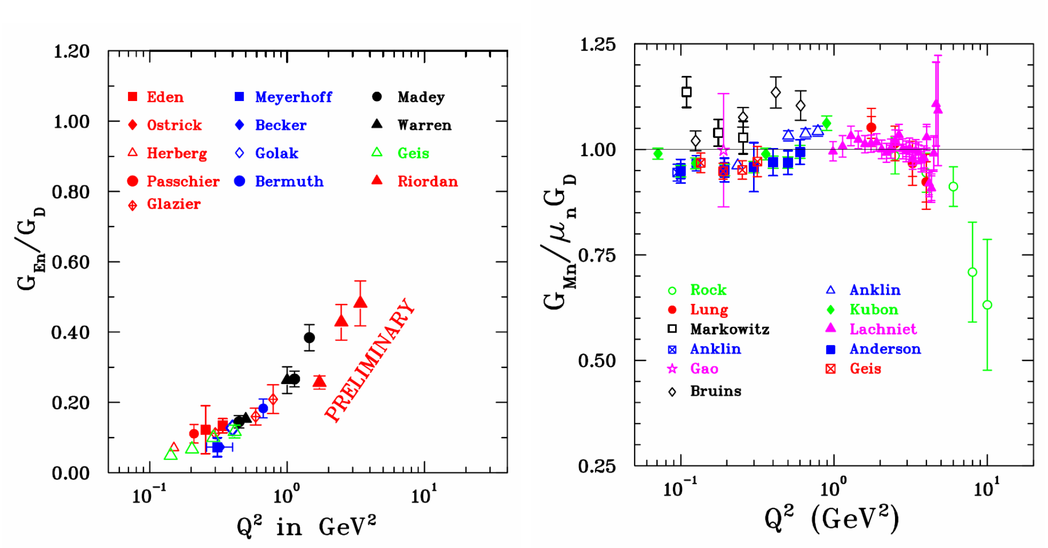

FIG. 27: Data for the neutron G_E and G_M obtained in double-polarization experiments [46].

The excitation spectrum of the nucleon is a feature of strong interaction in the non-perturbative domain. A variety of excited baryon resonances have been investigated in πN

elastic scattering and meson photoproduction experiments. The properties of these baryon resonances have been extracted, such as mass, width and branching ratios of their decay. The transition form factor from the nucleon to a baryon resonance B^* (NB^* form factor) is also a fundamental property of B^*. The transition form factors are defined similarly to the nucleon form factors, yet the final state is no longer a nucleon but a baryon resonance state B^*, and the matrix elements become $\langle B^*(p', s')|J_\mu|N(p, s)\rangle$. The first trial to determine the electromagnetic form factors for baryon resonances was done using inelastic electron scattering on protons at DESY [47]. Similar inelastic electron scattering experiments were carried out also at the Stanford Linear Accelerator Center (SLAC) [48]. The decay particles from the baryon resonances were not detected in these experiments and the form factors could be deduced only for the isolated excited resonance $\Delta(1232)P_{33}$. Recently, electromagnetic N^* transition form factors for many states have been obtained at JLAB/CLAS. Measurement of π^+ and $\pi^+\pi^-$ electroproduction on protons give the transition form factor of baryon resonances with a mass $W < 2.1$ GeV and a momentum transfer $Q^2 < 1.5$ GeV^2 [49, 50]. Figure 28 shows the form factor G^*_M for the $\gamma^* p \to \Delta(1232)P_{33}$ transition obtained at JLAB/CLAS.

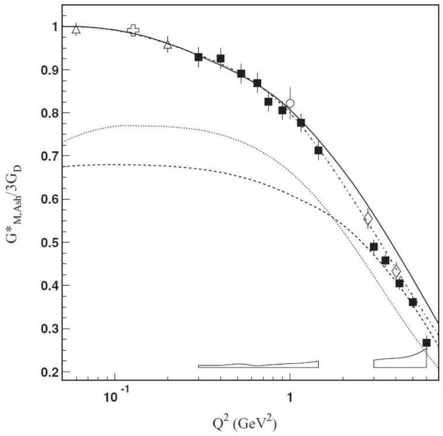

FIG. 28: Form factor G^*_M for the $\gamma^* p \to \Delta(1232)P_{33}$ transition relative to $3G_D$ [49].

The nucleon axial form factor can be defined with the axial current $A_\mu = \overline{\psi}\gamma_\mu\gamma_5\psi$ between the initial and final nucleons:

$$\langle N(p', s')|A_\mu|N(p, s)\rangle = \overline{u}(p', s')\left[\gamma_\mu\gamma_5 G_A(Q^2) + \frac{q_\mu\gamma_5}{2m}G_P(Q^2)\right]u(p, s). \qquad \text{(F4)}$$

The axial form factors characterize the distributions of the axial charge in hadrons at low Q^2 as a function of spatial resolving power. Pion exchange plays an important role in nuclear physics and thus the distributions of the axial charge, namely the current source of the coupling to pions, are important for understanding the hadron interaction. The Q^2 dependence of G_A for a nucleon can be determined by two types of experiments. One is quasi-elastic (QE) νN scattering ($\nu n' \to \mu^- p$), and the other is π^+ electroproduction on a proton ($ep \to e\pi^+ n$) [51]. The axial form factors are approximately described as

$$G_A(Q^2) = \frac{g_A}{\left(1 + \frac{Q^2}{M_A^2}\right)^2} \tag{F5}$$

with an axial mass M_A. Fitting to QE ν–N scattering experiments gives $M_A = 1.001 \pm 0.020$ GeV. M_A determined from π^+ electroproduction on a proton is 1.013 ± 0.015 GeV, which agrees well with M_A from QE ν-N experiments. Fig. 29 shows the axial masses obtained from these experiments. Recently, the axial form factors can be obtained by a lattice QCD calculation [52] and a direct comparison can be made between the experiments and the calculations.

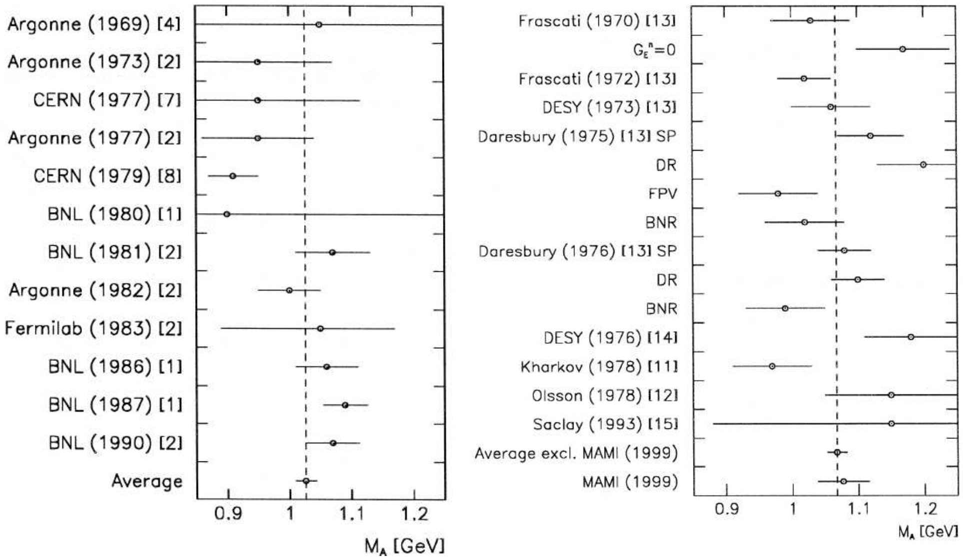

FIG. 29: Axial mass M_A extracted from quasi-elastic neutrino and antineutrino scattering experiments (left) and M_A extracted from charged pion electroproduction experiments (right) [51]. The dotted vertical lines indicate the average.

The axial NB^* transition form factors are defined similarly to the electromagnetic NB^* form factors with the matrix elements becoming $\langle B^*(p', s')|A_\mu|N(p, s)\rangle$. **We propose to determine the axial NB^* transition form factors for the first time from the Q^2 dependence of the B^* production yield coupling to virtual pions (kaons).** Since the axial form factors link the strong and weak interactions through the partial conservation of axial vector current (PCAC), they are important for both hadron and neutrino interactions [53].

As for the strangeness sector, the structure of the $\Lambda(1405)$ hyperon resonance is an important issue in hadron physics. Since $\Lambda(1405)$ is considered to be a quasi-bound state of $\bar{K}N$, its structure gives the $\bar{K}N$ interaction at low energies. The $\Lambda(1405)$ has a mass between the $\pi\Sigma$ and $\bar{K}N$ thresholds, and it decays to the $\pi\Sigma$ channel with $I = 0$ by the strong interaction. A dynamical description with coupled channels is required for understanding $\Lambda(1405)$. $\Lambda(1405)$ can be predominantly described by meson-baryon components in a coupled-channels approach based on chiral dynamics [57]. Recently, the possibility of two resonance state composition having a different coupling nature to the $\pi\Sigma$ and $\bar{K}N$ channels has been discussed for $\Lambda(1405)$ [56, 58–60]. Experimental efforts for understanding the $\Lambda(1405)$ nature were made by measuring the $\pi\Sigma$ invariant mass distributions for different $\pi\Sigma$ channels [61–64]. Since $\Sigma(1385)$ is located close to $\Lambda(1405)$, the decay particles from $\Lambda(1405)$ must be detected. We propose to determine the axial $p\Lambda(1405)$ transition form factors where the $\Lambda(1405)$ component is extracted from the isospin decomposition between the $\pi^- p \rightarrow K^{*0}X$ and $\pi^+ p \rightarrow K^{*+}X$ reactions.

2. Virtual Pions and Virtual Kaons

The virtual pions and kaons are realized by detecting the extremely forward produced vector mesons ρ and K^* at the high momentum secondary beamline at J-PARC. The t channel process is considered to be dominant for the pion-induced (π, ρ) and (π, K^*) reactions on a proton when the vector mesons ρ and K^* are detected at the extremely forward angles. The quantum numbers transferred to the proton target are the same as those for pseudo scalar mesons, namely virtual pions and kaons are considered to be exchanged. As for the non-strangeness sector, two different channels $\pi^- p \rightarrow \rho^0 X$ and $\pi^+ p \rightarrow \rho^0 X$ enable us to decompose the nucleon and Δ resonances. Both nucleon and Δ resonances are produced in the $\pi^- p \rightarrow \rho^0 X$ channel, and only the Δ resonance can be produced in the $\pi^+ p \rightarrow \rho^0 X$ channel. The mass of the produced baryon resonances is determined by a missing mass technique in the first stage experiment. We plan to identify the baryon resonance by detecting its decay particles in the second stage. As for the strangeness sector, two different channels $\pi^- p \rightarrow K^{*0}X$ and $\pi^+ p \rightarrow K^{*+}X$ enable us to decompose the Λ and Σ resonances. Both the Λ and Σ resonances are produced in the $\pi^- p \rightarrow K^{*0}X$ channel, and only the Σ resonance can be produced in the $\pi^+ p \rightarrow K^{*+}X$ channel. Figure 30 shows the diagrams for producing virtual pions and kaons.

Since the t channel exchange is considered, the cross section becomes smaller as the incident pion momentum increases. The acceptance of detecting the forward vector mesons with the charmed baryons spectrometer becomes higher since the decay particles from the vector mesons are boosted. The baryon mass resolution determined by the missing mass becomes worse since the momenta of the decay particles increases. Here, the acceptance of detecting the forward vector mesons at an incident momentum of 5 GeV/c has been estimated. The reactions of interest are $\pi^{\pm} p \rightarrow \rho^0 X$, $\pi^- p \rightarrow K^{*0}X$ and $\pi^+ p \rightarrow K^{*+}X$. The ρ^0, K^{*0} and K^{*+} mesons are assumed to be detected by $\pi^+\pi^-$, $K^+\pi^-$ and $K^0_s\pi^+ \rightarrow \pi^+\pi^-\pi^+$. The branching ratios of $\rho^0 \rightarrow \pi^+\pi^-$ and $K^{*0} \rightarrow K^+\pi^-$ are 100% and 67%, respectively. The

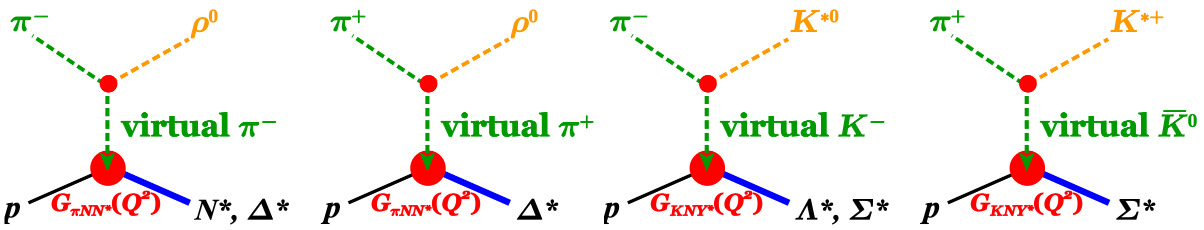

FIG. 30: Diagrams for producing virtual pions and kaons. The t channel process is considered to be dominant for the pion-induced (π, ρ) and (π, K^*) reactions on a proton when the vector mesons ρ (K^*) are detected at the extremely forward angles. The quantum numbers transferred to the proton target are the same as those for pseudo scalar mesons, namely virtual pions and kaons are considered to be exchanged.

branching ratio of $K^{*+} \to K^0\pi^+$ is 67%, the K_s component is 50% in K^0, the branching ratio of $K_s^0 \to \pi^+\pi^-$ is 69%. Therefore, the total branching ratio $K^{*+} \to \pi^+\pi^-\pi^+$ is expected to be 23%. These branching ratios are not taken into account in the acceptance estimation. Figure 31 shows the acceptance of detecting the forward vector mesons at 5 GeV/c as a function of the baryon mass for different momentum transfers t. The baryon mass resolution determined by the missing mass is worst for the $\pi^\pm p \to \rho^0 X$ reaction because the momenta of the decay particles from the vector meson are higher. In the $\pi^\pm p \to \rho^0 X$ reaction, a baryon mass resolution of approximately 10 MeV is expected with the charmed baryon spectrometer at an incident momentum of 5 GeV/c.

The produced vector meson ρ^0 at forward angles can be identified by detecting $\pi^+\pi^-$. Figure 32 shows the $\pi^+\pi^-$ invariant mass distribution for the $\pi^- p \to \pi^-\pi^+ n$ reaction at an incident momentum of 17.2 GeV/c [65]. The $\pi^+\pi^-$ shows a clear $\rho(770)$ peak together with $f_2(1270)$ and $\rho_3(1690)$ peaks. The differential cross sections for the $\pi^+ p \to \rho^0 \Delta^{++}$ reaction were measured at an incident momentum of 13.1 GeV/c. $\pi^+\pi^+\pi^- p$ final state events were obtained in the SLAC 82-inch bubble chamber. The differential cross section shows a strong forward peak as a function of $|t - t_{\rm min}|$ shown in Fig. 32. The slope is 20 GeV$^2/c^2$ and the value of the spin density matrix ρ_{00} is large (> 0.9) for $|t - t_{\rm min}| < 0.15$ GeV$^2/c^2$, which are well described well with a conventional pion exchange model with absorption.

Here, the strategy of determining the $G_{\pi NN^*}(Q^2)$ transition form factor is discussed. To extract $G_{\pi NN^*}(Q^2)$, the $\rho^0 \to \pi\pi$ transition form factor $G_{\rho\pi\pi}(Q^2)$ is necessary. $G_{\rho\pi\pi}(Q^2)$ can be deduced from the $\pi^- p \to \rho^0 n$ reaction because $G_{\rho\pi\pi}(Q^2)$ is common for different final state baryons for $\pi^\pm p \to \rho^0 X$ and because the axial form factors for a nucleon is well determined by QE νN scattering and π^+ electroproduction experiments. After $G_{\rho\pi\pi}(Q^2)$ is determined, the axial form factor can be determined as a function of produced baryon mass. In the second stage, we plan to detect the decay particles from the excited baryons; the axial form factor can then be determined for specific baryon resonances.

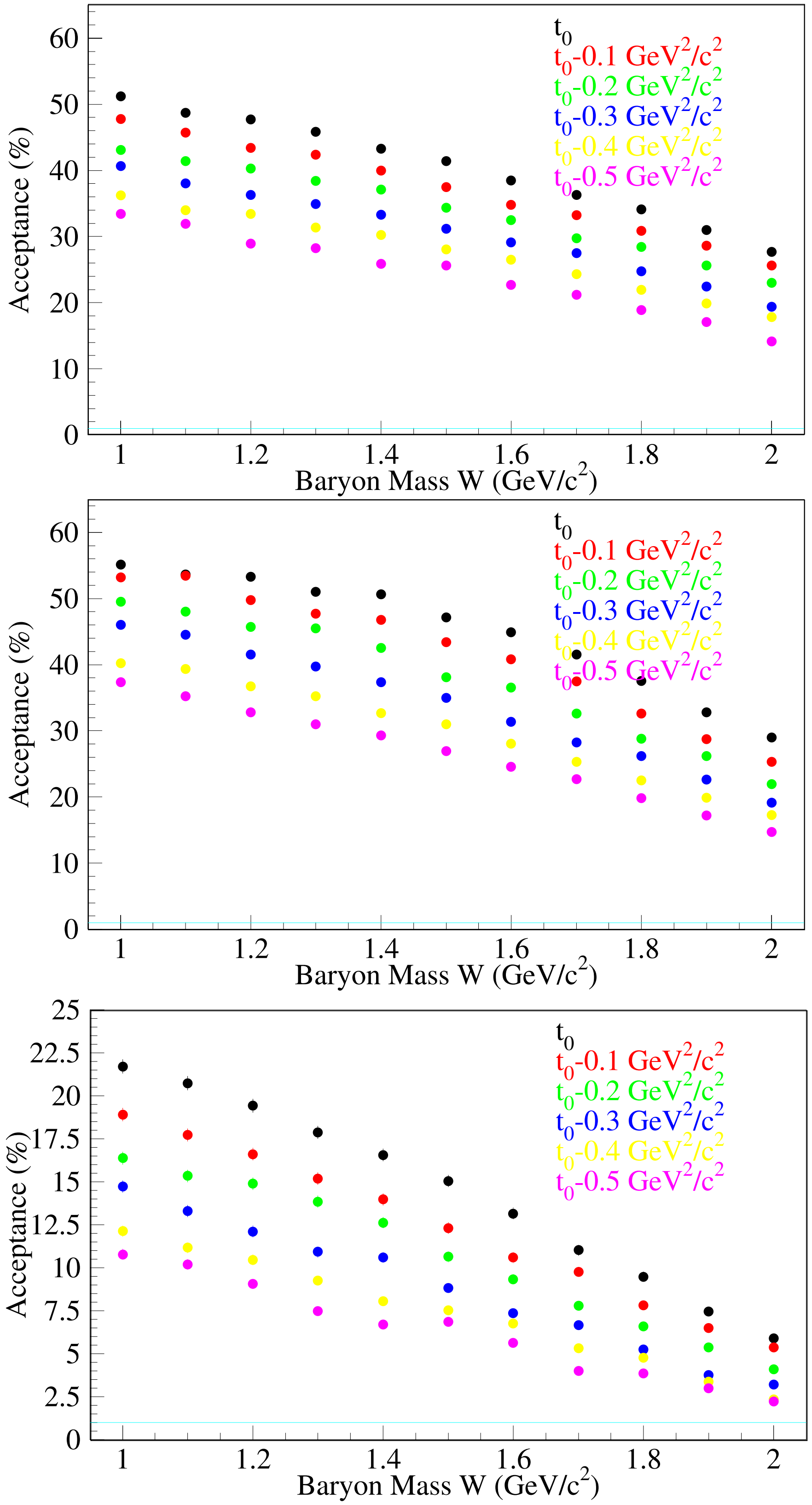

FIG. 31: Acceptance of detecting forward vector mesons at 5 GeV/c. The upper, central and lower panels show the acceptances as a function of produced baryon mass for the $\pi^{\pm}p \rightarrow \rho^0 X$, $\pi^- p \rightarrow K^{*0}X$ and $\pi^+ p \rightarrow K^{*+}X$ reactions. The ρ^0, K^{*0} and K^{*+} mesons are assumed to be detected by $\pi^+\pi^-$, $K^+\pi^-$ and $K^0_s\pi^+ \rightarrow \pi^+\pi^-\pi^+$. The branching ratios of $\rho^0 \rightarrow \pi^+\pi^-$, $K^{*0} \rightarrow K^+\pi^-$ and $K^{*+} \rightarrow K^0_s\pi^+ \rightarrow \pi^+\pi^-\pi^+$ are 100%, 67%, $67\% \times 50\% \times 69\% = 23\%$. However, they are not taken into account in the acceptance estimation. The color indicates the corresponding momentum transfer (Mandelstam variable t).

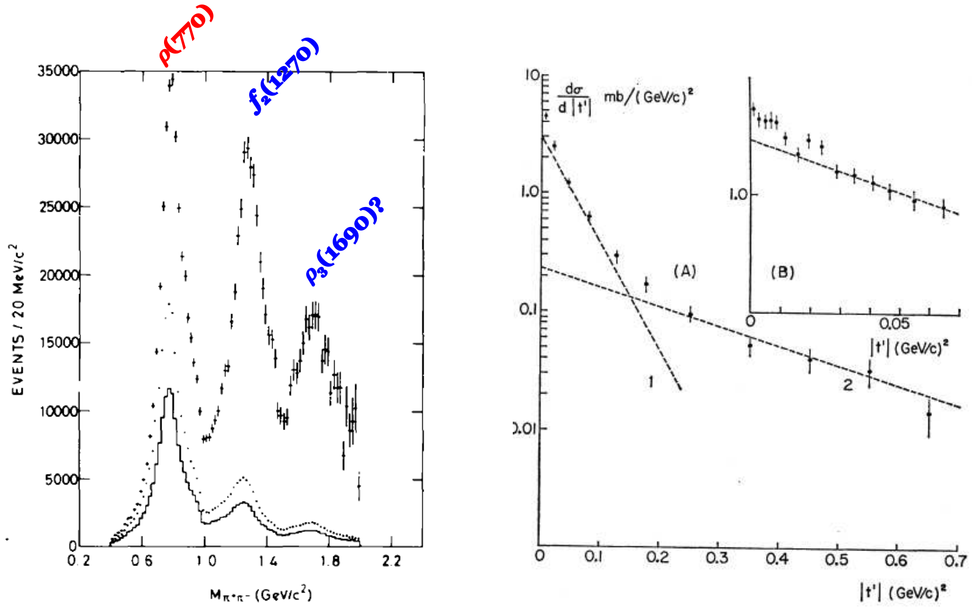

FIG. 32: $\pi^+\pi^-$ invariant mass distributions for events with $|t| < 0.15$ GeV$^2/c^2$ (left) [65]. The acceptance corrected number of events is shown by the points with error bars. Differential cross section as function of $|t'| = |t - t_{\rm min}|$ for the $\pi^+ p \to \rho^0 \Delta^{++}$ reaction at 13.1 GeV/c (right) [66] are also shown. The lines correspond to slopes of 20 and 3.8 GeV/c. The small $|t'|$ is plotted in the inset.

The similar $\pi^- p \to K^{*-} X$ reaction gives a transition form factor for a Θ^+ pentaquark baryon $G_{KN\Theta^+}$. Here, the K^{*-} meson is detected at forward angles, and it is identified by the $\bar{K}^0\pi^- \to (\pi^+\pi^-)\pi^-$ decay. Evidence for the pentaquark Θ^+ baryon was reported by the LEPS collaboration for the first time [67]. A narrow peak was observed in the K^+n invariant mass distribution for the $\gamma n \to K^- K^+ n$ reaction, and Θ^+ is a genuine exotic baryon predicted by Diakonov *et al.* [68]. The experimental situation for the existence of Θ^+ is controversial. Many collider experiments have found no positive evidence of the pK_s invariant mass distributions [69]. The CLAS collaboration searched for Θ^+ in the $\gamma p \to \bar{K}^0 K^+ n$ and $\gamma d \to pK^- K^+ n$ reactions [70]. No evidence for Θ^+ was obtained in these experiments, and only the upper limits for the Θ^+ productions were given. Other experiments by pion-, kaon- and proton-induced reactions showed no evidence for Θ^+ production: $\pi^- p \to K^- X$ [71], $K^+ p \to \pi^+ X$ [72] and $pp \to pK^0\Sigma^+$ [73] reactions. At this moment, three positive experiments exist: re-analysis of the $K^+{\rm Xe} \to K^0 p{\rm Xe}'$ reaction by the DIANA collaration [74], the $\gamma d \to K^+K^- pn$ reaction by the LEPS collaboration [75] and the $\gamma p \to K_s X$ reaction taken with the CLAS spectrometer by M.J. Amaryan *et al.* [76]. Since the Θ^+ production seems highly reaction dependent, the formation experiments of $K^+ n \to \Theta^+$ seem to clarify its existence. The K^+ beam with a momentum around 420 MeV/c is required for the formation experiments. Yet, it is difficult to obtain such a low momentum K^+ beam with a momentum analysis and particle identification since $c\tau = 3.712$ m for the K^+ meson and almost all the K^+ mesons decay before arriving at the target position. Therefore, a Θ^+ search by using the $\pi^- p \rightarrow K^{*-} X$ reaction is the best method. A small $K^* N \Theta^+$ coupling, which is suggested by the previous experiments, is not included in the $\pi^- p \rightarrow K^{*-} X$ reaction and the vertex is the same as the formation $K^0 p \rightarrow \Theta^+$.

[1] For example, see textbooks by F. Close, *An introduction to quarks and partons*, Academic Press, 1979; and also A. Hosaka and H. Toki, *Quarks, baryons and chiral symmetry*, World Scientific, 2001.

[2] M. Oka and K. Yazaki, Prog. Theor. Phys. **66**, 556 (1981); *ibid.* 572 (1981).

[3] J. Beringer *et al.*, Phys. Rev. D**86** (2012) 010001.

[4] R. L. Jaffe, Phys. Rev. D **15**, 267 (1977); R. L. Jaffe, Phys. Rev. D **15**, 281 (1977).

[5] M. Karliner and H. J. Lipkin, Phys. Lett. B **575**, 249 (2003) [arXiv:hep-ph/0402260].

[6] D. Jido, J. A. Oller, E. Oset, A. Ramos and U. G. Meissner, Nucl. Phys. A **725**, 181 (2003) [arXiv:nucl-th/0303062];
see also T. Hyodo and D. Jido, Prog. Part. Nucl. Phys. **67**, 55 (2012) [arXiv:1104.4474 [nucl-th]].

[7] M. Ida and R. Kobayashi, Prog. Theor. Phys. **36**, 846(1966).

[8] M. Anselmino *et al.* , Rev. Mod. Phys. **65**, 1199(1993).

[9] R. L. Jaffe, Phys. Rep. **409**, 1(2005).

[10] T. Friedmann, arXiv:0910.2229, 2009.

[11] C. Alexandrou, Ph. de Forcrand, and B. Lucini, Phys. Rev. Lett. **97**, 222002(2006).

[12] J. Green, M. Engelhardt, J. Negele, and P. Varilly, AIP Conf. Proc. **1441**, 172(2012).

[13] R. Mizuk *et al.* (Belle Collaboration), Phys. Rev. Lett. **98**, 262001(2007).

[14] H. Y. Cheng and C. K. Chua, Phys. Rev. **D75**, 014006(2007).

[15] J. H. Christenson *et al.* , Phys. Rev. Lett. **55**, 154(1985).

[16] A. B. Kaidalov, Z. Phys. C12, 63(1982); V.Yu Grishina *et al.* , Eur. Phys. J. **A25**, 141(2005); A. I. Titov and B. Kämpfer, Phys. Rev. **C78**, 025201(2008).

[17] Y. Nara: A Microscopic Transport Code for high energy nuclear collisions, http://quark.phy.bnl.gov/ ynara/jam/ ; Y. Nara *et al.* , Phys. Rev. **C61**, 024901(2000).

[18] J. W. Waters *et al.* , Nucl. Phys. **B17**, 445(1970).

[19] S. Yokkaichi *et al.*, "Electron pair spectrometer at the J-PARC 50-GeV PS to explore the chiral symmetry in QCD", the E16 proposal, June, 2006.
http://www.j-parc.jp/researcher/Hadron/en/Proposal_e.html#0606

[20] Urs Rohrer, Compendium of Transport Enhancements,
http://aea.web.psi.ch/Urs_Rohrer/MyWeb/trancomp.htm;
K. L. Brown, D. C. Carey, Ch. Iselin, and F. Rothacker, "Transport, a Computer Program for Designing Charged Particle Beam Transport Systems", CERN 73-16 (1973) and CERN 80-04 (1980).

[21] J. R. Sanford and C. L. Wang, BNL 11279 and BNL 11479, (1967).

[22] R. Mizuk *et al.*, Phys. Rev. Lett. **94**, 122002 (2005).

[23] N. Akopov *et al.*, Nucl. Instrum. Methods. A **479** 511 (2002).

[24] R. Honecker *et al.*, Nucl. Phys. B **13** 571 (1969).

[25] K. J. Foley *et al.*, Phys. Rev. Lett. **19**, 330 (1967).

[26] F. Barreiro *et al.*, Phys. Rev. D **17**, 669 (1978).

[27] K. Suetsugu, Master Thesis: "Performance of Pion, Kaon and Proton Identification with the Ring Imaging Čerenkov Couner of HERMES", Tokyo Institute of Technology, 2001.

[28] "Workshop on Physics at the High-momentum Beam Line of J-PARC", http://kds.kek.jp/conferenceDisplay.py?confId=9848, in Japanese, May, 2012.

[29] H. Kamano, A. Hosaka, T. Nakano, H. Noumi, T. Sato, K. Ozawa, S. Yasui, T. Hyodo, M. Oka, and D. Jido, An ancillary document to 'collected comments for the high momentum beam line'; "Construction of a High-resolution Charmed Particle Spectrometer at the HIgh-resolution, High-momentum Beam Line", submitted to the 14th PAC of J-PARC, March, 2012; In this document, interests of charmed barons are widely discussed. A part of the discussions are described again in Appendix A to D.

[30] K. H. Tanaka *et al.*, Nucl. Intrum. Meth. A**363**, 114(1995).

[31] N. Brambilla *et al.*, Eur. Phys. J. C **71**, 1534 (2011) [arXiv:1010.5827 [hep-ph]].

[32] A. V. Manohar and M. B. Wise, Camb. Monogr. Part. Phys. Nucl. Phys. Cosmol. **10**, 1 (2000).

[33] S. Yasui and K. Sudoh, Phys. Rev. D **80**, 034008 (2009) [arXiv:0906.1452 [hep-ph]].

[34] Y. Yamaguchi, S. Ohkoda, S. Yasui and A. Hosaka, Phys. Rev. D **84**, 014032 (2011) [arXiv:1105.0734 [hep-ph]].

[35] C.B. Dover and S.H. Kahana, Phys. Rev. Lett. **39**(1977) 1506.

[36] H. Bando and S. Nagata, Prog. Theor. Phys. **69** (1983) 557; H. Bando, Prog. Theor. Phys. **S81** (1985) 197.

[37] Y.R. Liu and M. Oka, Phys. Rev. **D85** (2012) 014015; W. Meguro, Y.R. Liu, M. Oka, Phys. Lett. **B704** (2011) 547.

[38] N. Suzuki, B. Julia-Diaz, H. Kamano, T. S. Lee, A. Matsuyama and T. Sato, Phys. Rev. Lett. **104**, 042302 (2010) [arXiv:0909.1356 [nucl-th]].

[39] V.Yu Grishina, L. A. Kondratyuk, W. Cassing, M. Mirazita, and P.Rossi, Euro. Phys. J. **A25**, 141(2005).

[40] A. I. Titov and B. Kämpfer, Phys. Rev. D**78**, 025201(2008).

[41] M. M. Brisudova, Euro. Phys. Jour. **A25**, 141(2001).

[42] F. Bumiller, M. Croissiaux, E. Dally, and R. Hofstadter, *Electromagnetic Form Factors of the Proton*, Physical Review **124**, 1623 (1961);

T. Janssens, R. Hofstadter, E. B. Huges, and M. R. Yearian, *Proton Form Factors from Elastic Electron-Proton Scattering*, Physical Review **142**, 922 (1966);

F. Borkowski, P. Peuser, G.G. Simon, V.H. Walther, and R.D. Wendling, *Electromagnetic form factors of the proton at low four-momentum transfer*, Nuclear Physics A **222**, 269 (1974);

F. Borkowski, P. Peuser, G.G. Simon, V.H. Walther, and R.D. Wendling, *Electromagnetic form factors of the peoton at low four-momentum transfer (II)*, Nuclear Physics B **93**, 461

(1975);

G.G. Simon, C. Schmitt, F. Borkowski, and V.H. Walther, *Absolute electron-proton cross sections at low momentum transfer measured with a high pressure gas target system*, Nuclear Physics A **333**, 381 (1980);

G.G. Simon, C. Schmitt, and V.H. Walther, *Elastic electric and magnetic e-d scattering at low momentum transfer*, Nucl. Phys. A **364**, 285 (1981);

W. Albrecht, H. J. Behrend, F.W. Brasse, W.F.H. Hultschig, and K.G. Steffen, *Elastic Electron-Proton Scattering at Momentum Transfers up to 245* F^{-2}, Physical Review Letters **17**, 1192 (1966);

W. Bartel, B. Dudelzak, H. Krehbiel, J.M. McElroy, U. Meyer-Berkhout, R.J. Morrison, H. Nguyen-Ngoc, W. Schmidt, and G. Weber, *Small-Angle Electron-Proton Elastic-Scattering Cross Sections for Squared Momentum Transfers Between 10 and 105* F^{-2}, Physical Review Letters **17**, 608 (1966);

D. Frerejacque, D. Benaksas, and D.J. Drickey, *Proton Form Factors from Observation of Recoil Protons*, Physical Review **141**, 1308 (1966);

W. Albrecht, H.-J. Behrent, H. Dorner, W. Flauger, and H. Hultschig, *Some Recent Measurements of Proton Form Factors*, Physical Review Letters **18**, 1014 (1967);

W. Bartel, B. Dudelzak, H. Krehbiel, J. M. McElroy, R.J. Morrison, W. Schmidt, V. Walther, and G. Weber, *Scattering of positrons and electrons from protons*, Physics Letters B **25**, 242 (1967);

W. Bartel, F.-W. Büsser, W.-R. Dix, R. Felst, D. Harms, H. Krehbiel, J. McElroy, J. Meyer, and G. Weber, *Measurement of proton and neutron electromagnetic form factors at squared four-momentum transfers up to 3 (GeV/c)*^{2}, Nuclear Physics B **58**, 429 (1973);

D. Ganichot, B. Grossetete, and D.B. Isabelle, *Backward electron-deuteron scattering below 280 MeV*, Nuclear Physics A **178**, 545 (1972);

P.N. Kirk *et al.*,, *Elastic Electron-Proton Scattering at Large Four-Momentum Transfer*, Physical Review D **8**, 63 (1973);

J.J. Murphy, Y.M. Shin, and D.M. Skopik, *Proton form factor from 0.15 to 0.79 fm*$^{-2}$, Physical Review C **9**, 2125 (1974);

C. Berger, V. Burkert, G. Knop, B. Langenbeck, and K. Rith, *Electromagnetic form factors of the proton at squared four-momentum transfers between 10 and 50 fm*$^{-2}$, Physics Letters B **35**, 87 (1971);

W. Bartel, F. Busser, W. Dix, R. Felst, D. Harms, H. Krehbiel, P. Kuhlmann, J. McElroy, and G. Weber, *Electromagnetic proton form factors at squared four-momentum transfers between 1 and 3 (GeV/c)*^{2}, Physics Letters B **33**, 245 (1970).

[43] J.J. Kelly, *Nucleon charge and magnetization densities from Sachs form factors*, Physical Review C **66**, 065203 (2002).

[44] G.A. Miller, *Shapes of the proton*, Physical Review C **68**, 022201(R) (2003).

[45] A.V. Belitsky, X. Ji and F. Yuan, *Quark imaging in the proton via quantum phase-space distributions*, Physical Review D **69**, 074014 (2004).

[46] Figures are given from Scholarpedia, the peer-reviewed open-access encyclopedia, Web site ⟨http://www.scholarpedia.org/article/Nucleon_Form_factors⟩.

[47] W. Bartel *et al.*, *The transverse and longitudinal cross sections for electroproduction of pions near the* $\Delta(1236)$*-isobar*, Physcs Letters B **27**, 660 (1968);
W. Bartel *et al.*, *Electroproduction of pions near the* $\Delta(1236)$ *isobar and the form factor* $G^*_M(q^2)$ *of the* $(\gamma N\Delta)$*-vertex*, Physcs Letters B **28**, 148 (1968).

[48] S. Stein *et al.*, *Electron scattering at* 4° *with energies of 4.5–20 GeV*, Physical Review D **12**, 1884 (1975).

[49] I.G. Aznauryan *et al.* (CLAS Collaboration), *Electroexcitation of nucleon resonances from CLAS data on single pion electroproduction*, Physical Review C **80**, 055203 (2009).

[50] V.I. Mokeev *et al.* (CLAS Collaboration), *Experimental study of the* $P_{11}(1440)$ *and* $D_{13}(1520)$ *resonances from the CLAS data on* $ep \to e'\pi^+\pi^-p'$, Physical Review C **86**, 035203 (2012).

[51] A. Liesenfeld *et al.*, *A measurement of the axial form factor of the nucleon by the* $p(e, e\pi^+)n$ *reaction at* $W = 1125$ *MeV*, Physics Letters B **468**, 20 (1999), and references therein.

[52] C. Alexandrou *et al.*, $\Delta(1232)$ *Axial Charge and Form Factors from Lattice QCD*, Physical Review Letters **107**, 141601 (2011).

[53] T. Sato, D. Uno, and T.-S.H. Lee, *Dynamical model of weak pion production reactions*, Physical Review C **67**, 065201 (2003).

[54] H. Budd, A. Bodek and J. Arrington, *Modeling Quasi-elastic Form Factors for Electron and Neutrino Scattering*, hep-ex/0308005 (Second International Workshop on Neutrino-Nucleus Interactions in the few-GeV Region NuInt02).

[55] E.J. Beise, *The Axial Form Factor of the Nucleon*, G0 Document 464-v1 (International Workshop on Parity Violation and Hadronic Structure PAVI/2004).

[56] P.J. Fink, Jr., G. He, R.H. Landau and J.W. Schnick, *Bound states, resonances, and poles in low-energy* $\bar{K}N$ *interaction models*, Physical Review C **41**, 2720 (1990).

[57] T. Hyodo, D. Jido and A. Hosaka, *Origin of resonances in the chiral unitary approach*, Physical Review C **78**, 025203 (2008).

[58] J.A. Oller and U.G. Meißner, *Chiral dynamics in the presence of bound states: kaon-nucleon interactions revisited*, Physics Letters B **500**, 263 (2001).

[59] D. Jido, A. Hosaka, J.C. Nacher, E. Oset and A. Ramos, *Magnetic moments of the* $\Lambda(1405)$ *and* $\Lambda(1670)$ *resonances*, Physical Review C **66**, 025203 (2002).

[60] D. Jido, J.A. Oller, E. Oset, A. Ramos and U.G. Meißner, *Chiral dynamics of the two* $\Lambda(1405)$ *states*, Nuclear Physics A **725**, 181 (2003).

[61] M. Niiyama *et al.*, *Photoproduction of* $\Lambda(1405)$ *and* $\Sigma^0(1385)$ *on the proton at* $E_\gamma = 1.5-2.4$ *GeV*, Physical Review C **78**, 035202 (2008).

[62] K. Moriya and R. Shumacher (CLAS collaboration), *Properties of the* $\Lambda(1405)$ *Measured at*

CLAS, Nuclear Physics A **835**, 325 (2010).

[63] I. Zychor *et al.*, *Lineshape of the hyperon measured through its decay*, Physics Letters B **660**, 167 (2008).

[64] G. Agakishiev *et al.* (HADES collaboration), *Baryonic resonances close to the* $\bar{K}N$ *threshold: the case of* $\Lambda(1405)$ *in pp collisions*, nucl-ex/1208.0205 (2012).

[65] G. Grayer *et al.*, *High Statistics Study of the Reaction* $\pi^- p \to \pi^- \pi^+ n$*: Apparatus, Method of Analysis, and General Features of Results at 17 GeV/c*, Nuclear Physics B **75**, 189 (1974).

[66] J.A. Gaidos, R.B. Willmann, J.W. Lamsa, C.R. Ezell, and F.T. Meiere, *Reaction* $\pi^+ p \to \rho^0 \Delta^{++}$ *at 13.1 GeV/c*, Physical Review D **1**, 3190 (1970).

[67] T. Nakano *et al.*, *Evidence for a Narrow* $S = +1$ *Baryon Resonance in Photoproduction from the Neutron*, Physical Review Letters **91**, 012002 (2003).

[68] D. Diakonov, V. Petrov, and M. Polyakov, *Exotic anti-decuplet of baryons: Prediction from chiral solitons*, Zeitschrift für Physik A **359**, 305 (1997).

[69] M.J. Longo *et al.* (HyperCP collaboration), *High statistics search for the* $\Theta^+(1.54)$ *pentaquark state*, Physical Review D **70**, 111101(R) (2004);

I. Abt *et al.* (HERA-B collaboration), *Limits for the Central Production of* Θ^+ *and* Ξ^{--} *Pentaquarks in 920-GeV pA Collisions*, Physical Review Letters **93**, 212003 (2004);

S. Schael *et al.* (ALEPH collaboration), *Search for pentaquark states in Z decays*, Physics Letters B **599**, 1 (2004);

J.Z. Bai *et al.*, *Search for the pentaquark state in* $\psi(2S)$ *and* J/ψ *decays to* $K_S^0 p K^- \bar{n}$ *and* $K_S^0 \bar{p} K^+ n$, Physical Review D **70**, 012004 (2004);

B. Aubert *et al.* (BABAR collaboration), *Search for Strange-Pentaquark Production in* e^+e^- *Annihilation at* $\sqrt{s} = 10.58$ *GeV*, Physical Review Letters **95**, 042002 (2005);

D.O. Litvintsev *et al.* (CDF collaboration), *Pentaquark Searches at CDF*, Nuclear Physics B — Proceedings Supplements **142**, 374 (2005);

Yu.M. Antipov *et al.*, *Search for* $\Theta(1540)^+$ *in the exclusive proton-induced reaction* $p+C(N) \to \Theta^+ \bar{K}^0 + C(N)$ *at the energy of 70 GeV*, Eurean Physical Journal A **21**, 455 (2004).

[70] R.De Vita *et al.* (CLAS collaboration), *Search for the* Θ^+ *pentaquark in the reactions* $\gamma p \to \bar{K}^0 K^+ n$ *and* $\gamma p \to \bar{K}^0 K_0 p$, Physical Review D **74**, 032001 (2006);

B. McKinnon *et al.* (CLAS collaboration), **Search for the Θ^+ Pentaquark in the Reaction** $\gamma d \to p K^- K^+ n$, Physical Review Letters **96**, 212001 (2006).

[71] K. Miwa *et al.*, *Search for* Θ^+ *via* $\pi^- p \to K^- X$ *reaction near production threshold*, Physics Letters B **635**, 72 (2006);

K. Shirotori *et al.*, *Search for the* Θ^+ *pentaquark via the* $\pi^- p \to K^- X$ *reaction at 1.92 GeV/c*, Physical Review Letters bf 109, 132002 (2012).

[72] K. Miwa *et al.*, *Search for the* Θ^+ *via the* $K^+ p \to \pi^+ X$ *reaction with a 1.2 GeV/c* K^+ *beam*, Physical Review C **77**, 045203 (2008).

[73] M. Abdel-Bary et al. (COSY-TOF collaboration), *Improved study of a possible* Θ^+ *production*

in the $pp \to pK^0\Sigma^+$ *reaction with the COSY-TOF spectrometer*, Physics Letters B **649**, 252 (2007).

[74] V.V. Barmin *et al.* (DIANA collaboration), *Observation of a baryon resonance with positive strangeness in* K^+ *collisions with Xe nuclei*, Physics of Atomic Nuclei **66**, 1715 (2003).

[75] T. Nakano *et al.*, *Evidence for the* Θ^+ *in the* $\gamma d \to K^+K^-pn$ *reaction by detecting* K^+K^- *pairs*, Physical Review C **79**, 025210 (2009).

[76] M.J. Amaryan *et al.*, *Observation of a narrow structure in* $p(\gamma, K_s)X$ *via interference with* ϕ*-meson production*, arXiv: 1110.3325 (2011);

M. Anghinolfi *et al.*, *Comment on the narrow structure reported by Amaryan et al*, arXiv: 1204.1105.